Master Thesis
Jan Grzegorzewski

Reaction-Diffusion Dynamics
With Fractional Brownian Motion

Winter term: 2016

Contents

Motivation

Anomalous diffusion can be observed in many different areas of nature, in particular, related to heterogeneous media like porous rocks, gels and crowded biological media with its prominent phenomena macromolecular crowding, confinement and macromolecular adsorption [1]. These environments exhibit remarkable characteristics like anomalous diffusion with its most popular power-law behaviour of the mean-square-displacement $(\delta r^2(t) \propto t^\alpha)$ [2], which violates the Einstein formula $\delta r^2(t) = 2dDt$ and thereby the central limit theorem. Anomalous diffusion is described by various theoretical models like the time random walks (CTRW) with an unconventional waiting time-distribution, the Lorentz models with excluded volume and a highly ramified remaining space or fractional Brownian motion (fBm). The latter is modelling a stochastic process with long-range correlations of the increments. fBm was first introduced as a family of Gaussian random functions by Mandelbrot and Van Ness in 1968 and motivated by examples in economics [3]. In contrast to different models of anomalous diffusion, the fBm approach is plainly phenomenologically defined by a power-law increase of the MSD and thus perfectly qualifies as a starting point to study effects arising from a power-law increase of the MSD.

This thesis focuses on the impact of fBm on enzymatic reaction kinetics in three-dimension space. Enzymes are large biological molecules, mostly proteins. Metabolic processes in cells rely vitally on enzymes. They help to break down large nutrient molecules like carbohydrates, fats and proteins during in the process of digestion. Other enzymes contrariwise help to form large and complex molecules from smaller once. Enzymes are involved in storage and release of energy, processes of respiration, vision, muscle contraction and transmission of nerve impulses. In fact, biochemical reactions are controlled mainly by enzymes. In general, they act as catalysts by lowering the activation energy. As stated by the Arrhenius law the activation energy is then increasing the reaction rates. The speed of reactions is typically increased by a factor of $10^6 - 10^{14}$. Pioneer work by Leonor Michaelis and Maud Menten [4] simplified enzymatic reaction kinetics and formulated a model based on the law of mass action. As one of the best known and important models of enzyme kinetics, it is of great interest to study effects from anomalous diffusion on Michaelis-Menten like reactions. For this purpose a particle-based simulation with an fBm integrator of a Michaelis-Menten like reactions was set up. Spatial and temporal effects arising from fBm were studied.

The thesis is organised into four chapters: The first chapter sets up theoretical foundations for fBm. Subsequently, fBm-generating algorithms are studied. Chapter 2 deals with models describing reactions in general but focuses on particle-based reaction-diffusion. A particle-based reaction-diffusion tool RevReaDDy, which served as a starting point for the implementation, is introduced. Chapter 3 focuses

more specifically on enzymatic reactions. A simulation model of an enyzmatic reaction with fBm is set up in RevReaDDy. Finally, results of the simulation are discussed and related to existing literature. Chapter 4 summarises the content of the thesis.

1 Fractional Brownian Motion

The Wiener process is a continuous-time stochastic process, which models white noise. It is applied to finance, biology, physics and much more if no or only weak correlations of the underlying processes are present. Brownian motion is the random motion of particles suspended in a fluid, which is modelled by a Wiener process. Velocities of particles, however, are always correlated at least for very short lag times in the physical world. It is often referred to as the super-diffusive regime. A $1\mu m$ silica bead in water for examples forgets its initial velocities in about $0.3ns$ within a corresponding displacement of about $1pm$ [5]. For longer times Brownian motion can be assumed.

Fractional Brownian Motion (fBm) is a more general family of stochastic Gaussian processes than standard Brownian motion with long-range correlations as its defining property. The main objective of this chapter is to explore the theoretical foundation for fBm, starting with Brownian motion in the following section. Further fBm-generating algorithms are introduced and analysed in terms of accuracy and performance.

1.1 Brownian Motion

Standard Brownian Motion (Bm) is a very important and well studied stochastic process. It describes the erratic motion of mesoscopic particles, which first were documented by Jan Ingenhousz in 1785, in particular for coal dust on the surface of alcohol [2]. Later on, in 1827 Robert Brown observed the erratic motion of pollen grains. Brownian motion has a Gaussian propagator, which has its origin in the Central Limit Theorem (CLT) for a sum of independent and identically distributed random variables (i.i.d.). Let's assume a set of N independent variables $\{X_j\}$ with a finite variance $\sigma_j^2 = \langle X_j^2 \rangle$ and the mean $\langle X_j \rangle = 0$. The definition of another random variable Y is given by:

$$Y = \frac{1}{\sqrt{N}} \sum_{j=1}^{N} X_j \tag{1.1}$$

This scenario in which a random variable is defined by the sum of another can be observed generically in nature. X_j are called increments of Y. The seemingly innocent assumption of independent increments result in a Gaussian distribution of

$\rho(y)$ in the limit of large N with $\rho(y)dy = \mathrm{P}(y < Y < y + dy)$:

$$\rho(y) = \frac{1}{\sqrt{2\pi}\sigma} \exp\left(-\frac{y^2}{2\sigma^2}\right) \tag{1.2}$$

A derivation of this very relevant result can be found in the appendix 5.1. Microscopic processes with i.i.d. velocities, have a Gaussian distribution for the overall change in position. Indeed, even the increments of Brownian motion are distributed Gaussian as a result of i.i.d. velocities at shorter time scales. A random walk in the limit of very small time steps, therefore, converges to Brownian motion.

With Bayes' theorem and an initial delta-distribution one can show that the transition probability $T_t(y|0) = \rho_t(y)$ is equivalent to the particle density distribution (see. appendix 5.2). The above-mentioned elaborations motivate processes with Gaussian transition probabilities. A process with a Gaussian distributed transition probability and independent increments is called Wiener process (Standard Brownian motion).

Brownian motion described by the Wiener process is a stochastic process $\{W_t\}$: $\Omega \rightarrow \mathbb{R}^d$ with $W_t(\omega)$ being the position of a particle with $\omega \in \Omega$ at time $t \in T$ in the observation time $T = [0, \infty)$. It has a fixed $x \in \mathbb{R}^d$ as its origin. The transition probabilities are [6]:

$$T_t(y|x) := (2\pi t)^{-d/2} exp\left(-\frac{||x - y||^2}{2t}\right) \qquad \text{for} \quad y \in \mathbb{R}^d, t > 0 \tag{1.3}$$

$$T_0(y|x) = \delta(x - y)$$

The Wiener process is a Gaussian process with mean $\langle W_t \rangle_y = x$ and particle position $W_o = x$ at $t = 0$. Its variance is $\langle W_t^2 \rangle_y = t$. It has stationary, independent, Gaussian increments. Following from the definition, Brownian motion has a property called Brownian scaling:

$$\{\hat{W}_t := \frac{1}{c} W_{c^2 t}\}_{t \geq 0} \tag{1.4}$$

A Wiener process has self-similar and fractal paths as a result from Brownian scaling.

However, it is a purely mathematical model with a missing connection to the strength of diffusion of a particle. The process, in fact, is a normalised diffusion process with the diffusion constant $D = \frac{1}{2}$. A mathematical description of diffusion was first realised by Fick in 1855 [7]. He applied partial differential equations for heat transfer, first solved by Fourier in 1822 [8]. Fick's second law of diffusion describes how diffusion causes the concentration $(c(\boldsymbol{r}, t))$ to change over time:

$$\frac{\partial}{\partial t} c(\boldsymbol{r}, t) = -\nabla J(\boldsymbol{r}, t) = D\Delta c(\boldsymbol{r}, t) \qquad \text{with} \qquad \Delta = \nabla^2 \tag{1.5}$$

With Fick's first law $J(\boldsymbol{r}, t) = -\nabla c(\boldsymbol{r}, t)$ and D defining the flux of particles and the diffusion coefficient, respectively. The notation of bold letters is chosen to describe

vectors (e.g. $\boldsymbol{r}$). Fick's first law results from the linear response theory. Fick's second law can be derived from mass conservation and Fick's first law. The most general form of mass conversation with a production term σ is described by the continuity equation:

$$\frac{\partial}{\partial t}c(\boldsymbol{r},t) = -\nabla J(\boldsymbol{r},t) + \sigma \tag{1.6}$$

Albert Einstein in 1905 proposed a similar equation to Fick's second law of diffusion, to solve one-dimensional Brownian motion [9]. This was the first derivation and application of probabilistic stochastic theory. Derived from the kinetic gas theory and a statistical description of collisions, in 1906 Marian von Smoluchowski could give similar results to Einstein [10]. The concentration $c(\boldsymbol{r},t)$ is proportional to the transition probability $\mathrm{P}(\boldsymbol{r},t) \propto c(\boldsymbol{r},t)$, with $\int d\boldsymbol{r}\mathrm{P}(\boldsymbol{r},t) = 1$. The transition probability of the Wiener process builds the foundation for a more physical description of particle motion by a propagator:

$$\mathrm{P}(r,t) = (4\pi Dt)^{-d/2} \exp\left(-\frac{r^2}{4Dt}\right) \tag{1.7}$$

The propagator $\mathrm{P}(r,t)$ can be interpreted as the probability to move a distance r during a time t. d is the dimension of the space of $\boldsymbol{r}$. One can show that this propagator is, in fact, solving the diffusion equation eq. (1.5) with the meaningful initial condition of vanishing concentration at boundaries (see. appendix 5.3):

$$c(\pm\infty, t) = 0 \tag{1.8}$$

The most important property of Brownian motion in the context of this thesis, is the mean square displacement $(\delta r^2(t))$, which grows linearly with the number of steps:

$$\delta r^2(t) = <[\boldsymbol{R}(t) - \boldsymbol{R}(0)]^2> = 2dDt \tag{1.9}$$

Here, $\boldsymbol{R}(t)$ is the position of the particle at time t. Brownian scaling was mentioned as a property of a Wiener process. It obviously also applies as a property to the propagator of Brownian motion. A scale-free form of the Gaussian propagator exists as a more intuitive consequence of Brownian scaling:

$$\mathrm{P}(r,t) = r^{-d}\mathcal{P}_{gauss}(\hat{r}) \tag{1.10}$$

$$\text{with} \quad \hat{r} = \frac{r}{\sqrt{2Dt}} \quad \text{and} \quad \mathcal{P}_{gauss}(\hat{r}) = (2\pi)^{-d/2}\hat{r}^d \exp\left(-\frac{\hat{r}^2}{2}\right) \tag{1.11}$$

The scale free form of Bm can later on be compared to the scale free form of fractional Brownian motion, which will be introduced next. This property results in a neat possibility of analysis of Bm- and fBm-generating algorithms later on.
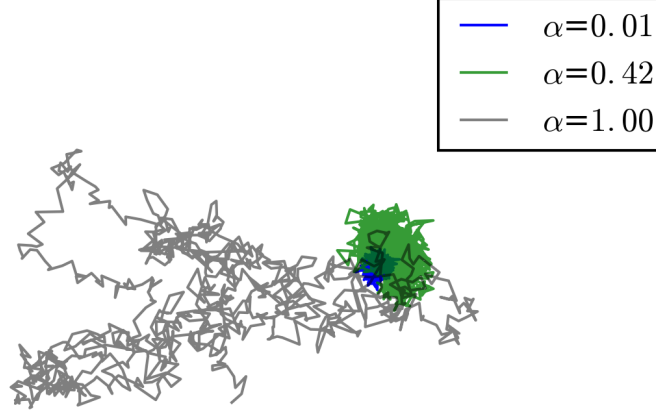
Figure 1.1: Three, three-dimensional fBm trajectories for an anomalous coefficient in the range of $0.01 \leq \alpha \leq 1$, generated by the Lowen algorithm are shown. The general diffusion constant, the time step and trajectory length were chosen as follows: $K_\alpha = 1$, $\Delta t = 1$, $M = 1000$.

1.2 Fractional Brownian Motion

In the previous section, the MSD has been shown to be linear with time as a result of the central limit theorem. In normal liquids, this behaviour can be seen already at time scales higher than picoseconds [2]. Nevertheless, many experiments show a power law behaviour of the MSD ($\delta r^2(t) \propto t^\alpha$ for $0 < \alpha < 1$) over certain time windows from microseconds to even seconds. Thus, the central limit theorem does not hold, at least in these time scales. It can be shown that persistent correlations of the increments are present. In soft matter, like polymers, a sub-diffusive behaviour is typically present in a time window but finally, the linear MSD takes over. Fractional Brownian motion idealises this situation by imposing that the central limit theorem is violated for all time scales. The basic feature of fBm is that the "span of interdependence" between their increments can be said to be infinite [3].

Just like the Wiener process, continuous-time Fractional Brownian motion (ctfBm) is a continuous-time Gaussian process $\{B_t^\alpha\} : \Omega \to \mathbb{R}^d$ at time $t \in T$ in the observation time $T = [0, \infty)$. It is fully specified by its mean $\langle B_t \rangle = 0$ and its covariance function:

$$\text{Cov}[B_t^\alpha, B_s^\alpha] = \frac{\sigma^2}{2}[t^\alpha - 2(s-t)^\alpha + s^\alpha] \qquad \text{for} \qquad t < s \qquad (1.12)$$

With the mean and the covariance defined, the mean square displacement for fBm can be derived as:

$$\langle (B_t^\alpha - B_s^\alpha)^2 \rangle = (s-t)^\alpha \sigma^2 \qquad (1.13)$$

Fractional Brownian motion exhibits a power law behaviour of the mean square dis-

placement and therefore, indeed motivates to act as a model for anomalous diffusion.

Fractional Brownian motion can be alternatively expressed in terms of its incremental sequence. The incremental sequence is a related stochastic process called continuous-time fractional Gaussian noise (ctfGn). CtfGn is a continuous-time Gaussian process $\{X_t^\alpha\} : \Omega \to \mathbb{R}^d$ at time $t \in T$ in the observation time $T = [0, \infty)$. The mean is zero $\langle X_t^\alpha \rangle = 0$ and variance $\text{Var}[X_t^\alpha] = \langle (X_t^\alpha)^2 \rangle = \sigma^2$:

$$B_t^\alpha = \int_s^t X_{t'}^\alpha dt' + B_s^\alpha \qquad \text{for} \qquad t < s \tag{1.14}$$

The covariance function for ctfGn can be derived from the covariance function of fractional Brownian motion:

$$\text{Cov}[X_t^\alpha, X_s^\alpha] = \frac{d^2}{dtds}\text{Cov}[B_t^\alpha B_s^\alpha] = \sigma^2 \frac{d^2|t-s|^\alpha}{dtds} \tag{1.15}$$

$$= \alpha(\alpha-1)\sigma^2|t-s|^{\alpha-2} + \alpha\sigma^2|t-s|^{\alpha-1}\delta(t-s) \tag{1.16}$$

The first term of this covariance function is describing the correlation of the increments. For Wiener white noise ($\alpha = 1$) the first term disappears and the second reduces to:

$$\text{Cov}[X_t, X_s] = \sigma^2\delta(t-s) \tag{1.17}$$

The description of fractional Brownian motion in terms of fractional Gaussian noise is often convenient because of fGn's stationarity. It is possible to apply the Wiener-Khinchin theorem on a stationary random process. Thus, a spectral decomposition exists. The Wiener-Khinchin theorem states that, the power spectral density can be written as the Fourier transform of the auto-covariance function:

$$S(\omega) = \int_{-\infty}^\infty \text{Cov}[X_t, X_0]\exp[-2\pi i\omega t]dt \tag{1.18}$$

The power spectral density for fGn for $\omega \longrightarrow 0$ can be written as [2]:

$$S(\omega)_{fGn} = \sigma^2\Gamma(1+\alpha)(-i\omega)^{1-\alpha} \tag{1.19}$$

For the Wiener white noise ($\alpha = 1$), the result simplifies to a constant:

$$S(\omega)_{Gn} = \sigma^2 \tag{1.20}$$

For fBm-generating algorithms, the discrete time version of fractional Brownian motion (fBm) and Gaussian noise (fGn) are interesting as well. The relation between them can be written as:

$$B_t^\alpha = \sum_{i=0}^k X_{t_i}^\alpha \qquad \text{with} \qquad t_i = t_0 + i\Delta t \tag{1.21}$$

The covariance function of discrete time fractional Gaussian noise is:

$$\text{Cov}[X_n^\alpha, X_m^\alpha] = \langle (B_{n+1}^\alpha - B_n^\alpha)(B_{m+1}^\alpha - B_m^\alpha) \rangle$$
$$= \frac{\Delta t^\alpha \sigma^2}{2}[(n - m - 1)^\alpha - 2(n - m)^\alpha + (n - m + 1)^\alpha] \qquad (1.22)$$
$$\text{for} \quad n \geq m$$

Due to stationarity one can write the auto-covariance function as:

$$\text{Cov}[X_0^\alpha, X_n^\alpha] = \frac{\Delta t^\alpha \sigma^2}{2}[(n - 1)^\alpha - 2n^\alpha + (n + 1)^\alpha] \qquad (1.23)$$

A more detailed study of fBm and fGm can be found in [11].

Similar to the line of argument for Brownian motion, also fBm needs a connection to the strength of diffusion. This connection is introduced by the variance of fGn as:

$$\sigma^2 = 2dK_\alpha \qquad (1.24)$$

The mean square displacement for fBm follows from eq. (1.13) as:

$$\delta r^2(t) = 2dK_\alpha t^\alpha \qquad (1.25)$$

Here, $K_\alpha > 0$ is the generalised diffusion coefficient of the physical dimension $\text{cm}^2/\text{sec}^\alpha$. The more physical description in terms of a propagator is the correlation function of the single particle density $P(\boldsymbol{r} - \boldsymbol{r}', t - t') = V\langle \rho(\boldsymbol{r}, t)\rho(\boldsymbol{r}', t') \rangle$. Here, the single particle density $\rho(\boldsymbol{r}, t) = \langle \delta(\boldsymbol{r} - \boldsymbol{R}(t)) \rangle$ describes the density of a particle, which is localised at position $\boldsymbol{R}(t)$. V is the volume. Just like Brownian motion, fractional Brownian motions increments $\Delta\boldsymbol{R}$ are Gaussian distributed with zero mean. The single particle density results in:

$$P(\boldsymbol{r}, t) = [4\pi K_\alpha t^\alpha]^{-d/2} \exp\left[\frac{-|\boldsymbol{r}|^2}{4K_\alpha t^\alpha} \right] \qquad (1.26)$$

The propagator of fBm can be transformed into a scale-free form. A scale-free form will be relevant in the analysis of the algorithm. It is related to the scale-free form of standard Brownian motion (see eq. (1.11)):

$$P(\boldsymbol{r}, t) = \boldsymbol{r}^{-d}\mathcal{P}_{gauss}(\hat{\boldsymbol{r}}) \qquad (1.27)$$

$$\text{with} \quad \hat{\boldsymbol{r}} = \frac{\boldsymbol{r}}{\sqrt{2K_\alpha t^\alpha}} \quad \text{and} \quad \mathcal{P}_{gauss}(\hat{\boldsymbol{r}}) = (2\pi)^{-d/2}\hat{\boldsymbol{r}}^d \exp\left(-\frac{|\hat{\boldsymbol{r}}|^2}{2} \right) \quad (1.28)$$

Velocities ($\boldsymbol{\xi}(t)$) in the physical world can be described by fractional Brownian noise. The velocity auto-correlation function (VACF) ($Z(t)$) can be expressed from the

auto-covariance function of fGn as defined in eq. (1.15):

$$Z(|t - t'|) = \frac{1}{d} \langle \boldsymbol{\xi}(t) \bullet \boldsymbol{\xi}(t') \rangle = \frac{1}{2d} \frac{d^2}{dt^2} \delta r^2(t - t') \tag{1.29}$$

The frequency representation of the velocity auto-correlation function of fractional Brownian motion is defined analogously to eq. (1.19) as:

$$\tilde{Z}(\omega) = K_\alpha \Gamma(1 + \alpha)(i\omega)^{1-\alpha} \tag{1.30}$$

For the analysis of fBm-generating algorithms an indicator, if the created increments indeed are Gaussian, will be of interesting. One can show that for Gaussian propagators with zero-mean, all but the second cumulants vanish. For non-Gaussian transport also further cumulants are non-zero. The cumulants can be obtained by expanding the characteristic function of $\Delta R(t)$ for small wave numbers $k \to 0$. Its logarithm returns the cumulants. From the cumulants, the so-called non-Gaussian parameter can be defined [2]:

$$\text{NGP}(t) = \frac{d\delta r^4(t)}{(d+2)[\delta r^2(t)]} - 1 \tag{1.31}$$

The non-Gaussian parameter reveals non-Gaussian transport if $\text{NGP}(t) > 0$. This, in turn, does not lead to sure Gaussian transport for $\text{NGP}(t) = 0$. Cumulants of higher order still can be non-zero.

1.3 Algorithm

Effects of anomalous diffusion increase their relevance for long times. Thus, a fractional Brownian motion generating algorithm for preferably long trajectories is going to be searched for. Exactness and performance of the algorithm matter. In literature, several algorithms are described. Promising exact methods are: Cholesky [12], Hosking [13], Davis-Harte [12] and Lowen [14] method. Cholesky method claims to perform $\mathcal{O}(M^3)$ with the length of trajectory M and $\mathcal{O}(M^2)$ for every next trajectory. Davis-Harte and Lowen method claim to be exact and fast $\mathcal{O}(Mlog(M))$ [15][14]. There are further algorithms with even faster performance (e.g. the $RMD_{3,3}$- method [12] with $\mathcal{O}(M)$) . However, they are approximations. In order to choose an algorithm, four algorithms were analysed in terms of accuracy and speed. 1.Cholesky 2. Davis-Harte 3.Lowen and 4. an own naive algorithm. All the methods are based on one or the other correlation functions described in the previous section.

Cholesky Method

The Cholesky method [12] is based on the auto-covariance function of fGn as described by eq. (1.12). The algorithm is shown in table 1.1. This approach is simple but as claimed by Dieker [12] unfortunately not efficient with an algorithmic scal-

1. Calculate the covariance matrix of fGn:

$$\Gamma = (\text{Cov}[x_i, x_j]) \quad , \tag{1.32}$$

$$\text{Cov}[x_i, x_j] = \Delta t^\alpha \sigma^2 (i^\alpha + j^\alpha - |i - j|^\alpha)/2 \tag{1.33}$$

2. Calculate the eigenvalues λ and eigenvectors $\boldsymbol{v}$ of Γ

3. Compute Σ the square root of Γ by the eigenvalues.

4. Draw for every entrance of the vector $\boldsymbol{\eta}$ a standard Gaussian distributed random number. Length of the vector is defined by the length M of the trajectory:

$$\eta_k = \mathcal{N}(0,1) \quad , \qquad k = 0, 1, 2, ..., M \tag{1.34}$$

5. Calculate the fGn by $B_k^\alpha = \Sigma \boldsymbol{\eta_k}$.

Table 1.1: The table shows Choleskys fBm-generating method.

ing of $\mathcal{O}(M^3)$ with the trajectory length (M). Performance and accuracy of all algorithms are discussed in detail in the last two sections of the chapter.

A Naive Algorithms

In this section, a naive algorithm based on the VACF in the frequency domain is introduced. This was the first attempt of a fast fBm algorithm, without any insight from the existing literature. The idea is to compute the increments in the frequency domain and eventually transform them back to the time domain. The algorithm is described in table 1.2. In the first step of the algorithm, four times the number of increments in comparison to the trajectory length are generated. It counteracts a problem arising from the boundary problem of the FFT. The problem is visualised in fig. 1.2. The figure shows an ensemble-averaged mean square displacement for $\alpha = 0.5$ for two versions of the algorithm. One curve in the figure is for the algorithm with a modification introduced in step 4. The other is for now of interest. It can be seen that on average all the particles travel back to their initial position. It is not shown in the plot, however, this is even true for every trajectory. The FFT has a downside compared to the continuous Fourier transform, which causes this effect. The VACF is zero at zero-frequency $\tilde{Z}_{l=0} = 0$. From eq. (1.37) also the first increment in the frequency domain is zero $\tilde{\xi}_{l=0} = 0$. Due to eq. (1.36) also the

1. Generate $4M$ independent normally distributed random increments:

   $$\eta_k \sim \mathcal{N}(0, \sqrt{\Delta t}) \quad , \qquad k = 0, 1, 2, ..., 4M \tag{1.35}$$

2. Fourier transform the increments via FFT into the frequency domain:

   $$\tilde{\eta}_l = \sum_{k=0}^{4M-1} \eta_k \exp\left[\frac{-i2\pi lk}{4M}\right] \Delta t \quad , \qquad l = 0, 1, 2, ..., 4M \tag{1.36}$$

3. Generate fractional increments in the frequency domain with the VACF:

   $$\tilde{\xi}_l = \tilde{\eta}_l \sqrt{2Re(\tilde{Z}_l)} \tag{1.37}$$

   Here, $\tilde{Z}_l$ is the discrete VACF in the frequency domain:

   $$\tilde{Z}_l = K_\alpha \Gamma(1+\alpha)(i2\pi l\Delta\omega)^{1-\alpha} = K_\alpha \Gamma(1+\alpha)\left(\frac{il2\pi}{4M\Delta t}\right)^{1-\alpha} \tag{1.38}$$

4. Replace the zero-increment in the frequency domain with:

   $$\tilde{\xi}_{l=o} = \mathcal{N}(0, \sqrt{2K_\alpha(4M\Delta t)^\alpha}) \tag{1.39}$$

5. Reverse Fourier transform the increments into the time domain:

   $$\xi_k = \frac{1}{4M} \sum_{l=0}^{4M-1} \tilde{\xi}_l \exp\left[\frac{2\pi ilk}{4M}\right] \Delta\omega \tag{1.40}$$

6. Build the cumulative sum only for the first quarter of the total number of generated increments:

   $$B_n^\alpha = \sum_{k=0}^{n-1} \xi_k, \qquad n = (0, 1, .., M) \tag{1.41}$$

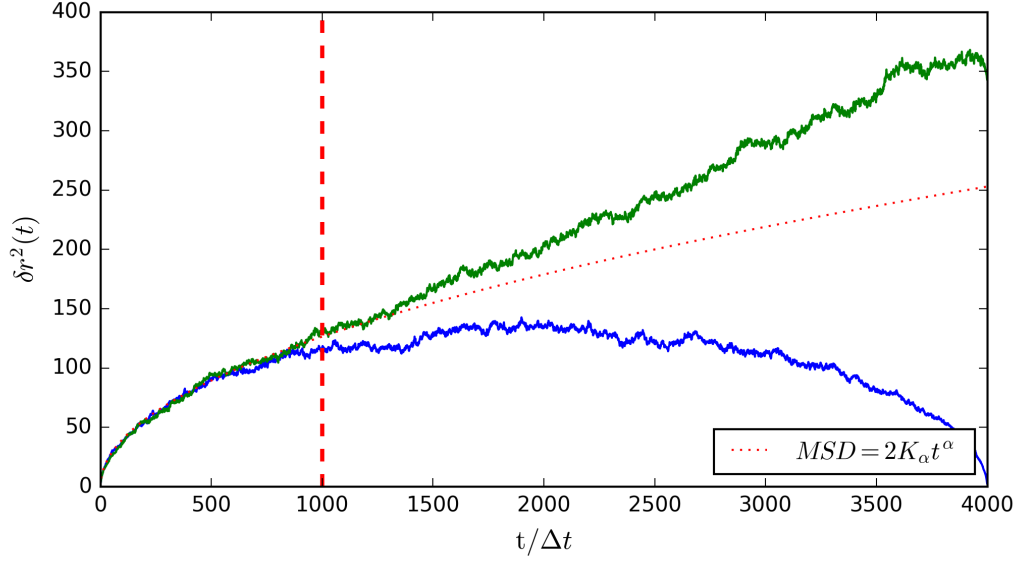Table 1.2: The table shows a naive fBm-generating algorithm.

Figure 1.2: An ensemble-average mean square displacement of two versions of the naive algorithm. The green curve is the MSD of the algorithm with the correction introduced in step 4 and the blue curve without.

following relation holds:

$$\tilde{\xi}_{l=0} = \sum_{k=0}^{M-1} \xi_k e^0 \Delta t = \Delta R_M \tag{1.42}$$

ΔR is the distance between the starting point and the position of the particle. Therefore, the particle would travel after M steps back to its initial position. The naive idea is to generate a trajectory four times longer than the desired length and only take the first forth into consideration. This can be thought of as a finite-time correction. The cut is displayed as a vertical red dashed line. The plot suggests not a perfect but at least a better agreement of the generated data to the theoretical mean square displacement for short times. Hereafter, normally distributed random numbers are transformed into the frequency domain. Wiener-Khinchin's theorem suggests to multiply the random numbers with the square root of two times the VACF. Besides taking only one-quarter of the trajectory a modification to the algorithm was introduced in step 4. Its impact in the MSD is shown in fig. 1.2 as the green line. Instead of accepting eq. (1.42), the zero-frequency increment is calculated as follows:

$$\tilde{\xi}_{l=0} = \mathcal{N}(0, \sqrt{2K_\alpha (M\Delta t)^\alpha}) \tag{1.43}$$

This equation would be correct if we assumed fractional Brownian motion to be a Markovian process. This is certainly is not the cause. This approximation seems

to improve the accuracy only slightly. Finally in step 4 the increments are back transformed into the time domain and in step 5 the cumulative sum of fGn is calculated, which yields fBm. The described algorithm can be performed independently for every Cartesian component for three-dimensional fractional Brownian motion. Different Cartesian components are independent. Without any extensive analysis of the naive algorithm one can already conclude draw backs in terms of convergence close to the overall simulation time.

Lowen Algorithm

1. Compute the auto-covariance function R_n^ξ of a periodic stochastic process ξ_n:

$$R_n^\xi = \begin{cases} \frac{1}{2}\left[1 - \left(\frac{n}{N}\right)^\alpha\right] & \text{for } 0 \le n \le M \\ R_{2M-n}^\xi & \text{for } M \le n \le 2M \end{cases} \tag{1.44}$$

2. Transform the auto-covariance function via FFT. The result is called the spectral density of the stochastic process ξ_n:

$$S_k^\xi = \text{FFT}(R_n^\xi; k) \tag{1.45}$$

3. Calculate $\tilde{\xi}_k$ the Fourier transform of the stochastic process ξ_n:

$$\tilde{\xi}_k = \begin{cases} 0 & \text{for } k = 0 \\ \exp(i\theta_k)\eta_k\sqrt{S_k^\xi} & \text{for } 0 \le k \le M \\ \eta\sqrt{S_k^\xi} & \text{for } k = M \\ \tilde{\xi}_{2M-k}^* & \text{for } M \le k \le 2M \end{cases} \tag{1.46}$$

$\{*\}$ denotes the complex conjugate, θ_k is a random phase uniformly distributed in $(0, 2\pi]$. η_k is a random Gaussian variable with zero mean and variance 1 $[\eta_k \sim \mathcal{N}(0,1)]$.

4. Perform the inverse Fourier transform on $\tilde{\xi}_k$ and use the first half of the resulting stochastic process ξ_n multiplied by a factor:

$$\xi_n = \frac{\text{FFT}^{-1}(\tilde{\xi}_k; n)}{2M} \tag{1.47}$$

$$B_n^\alpha = \sqrt{2K_\alpha M^\alpha \Delta t^\alpha}(\xi_n - \xi_0) \qquad \text{for} \quad 0 \le n \le M \tag{1.48}$$

Table 1.3: The table shows Lowen fBm-generating algorithm [14].

An algorithm by Lowen [14] was implemented. Lowen algorithm claims to be both fast ($\mathcal{O}(NlogN)$) and exact. However, our implementation shows not to be exact, which is shown in the analysis part. It starts with a auto-covariance function R_n^ξ. Its second derivative yields the auto-covariance of discrete time fGn described by eq. (1.23). R_n^ξ can be thought of as an auto-covariance function of a stationary periodic version of fBm. Lowen algorithm is described in table 1.3. Let's check the auto-covariance function of B_n^α resulting from the algorithm:

$$Cov[B_n^\alpha, B_m^\alpha] = 2K_\alpha \Delta t^\alpha N^\alpha \langle (\xi_n - \xi_0)(\xi_m - \xi_0) \rangle \tag{1.49}$$

$$= 2K_\alpha \Delta t^\alpha N^\alpha \langle \xi_n \xi_m \rangle - \langle \xi_0 \xi_m \rangle - \langle \xi_0 \xi_n \rangle + \langle \xi_0^2 \rangle \tag{1.50}$$

$$= K_\alpha \Delta t^\alpha [n^\alpha - 2(m-n)^\alpha + m^\alpha] \qquad \text{for} \qquad n < m \tag{1.51}$$

The auto-covariance function indeed satisfies the condition for fBm with variance similar to eq. (1.24). In step 3 the phase and amplitude of the Fourier transform ξ_m were chosen to be random as suggested in [16]. The second derivative of $R_\xi(n)$ is positive. $R_\xi(n)$ results in a periodic function with non-negative curvature. Its Fourier transform S_k^ξ is, real, symmetric and non-negative for all k. S_k^ξ is then a valid power spectral density function of the discrete-time periodic process ξ_n with period $2M$ and R_n^ξ its valid auto-covariance function [14]. This algorithm is actually using the property of Brownian scaling eq. (1.4) to generate a realisation of fBm with non-negative auto-covariance function.

Davis-Harte Algorithm

Davis-Harte algorithm [15] is related to Lowen Algorithm. It is also based on a FFT. The author claims the algorithm to be exact and its performance to scale with the length of the trajectory as ($\mathcal{O}(NlogN)$) . However, in contrast to Lowen algorithm, it is based on the covariance function of fGn described by equation eq. (1.23). Thus, it actually generates the increments of fBm. The algorithm is shown in table 1.4.

Accuracy Analysis

The algorithms were implemented in Python and C++. For the C++ implementation, a wrapper to Python was added. All algorithms were analysed by an analysis class. The C++ implementation is using the FFTW library for the Fast Fourier Transform [17] and Mersenne-Twister (gsl_rng_mt19937) [18] as the random number generator. Python implementations were developed beforehand and only serve as a reference. Python uses the numpy.fft library for the Fast Fourier Transform and also the Mersenne-Twister random number generator.

Insights of stochastic algorithms can be obtained by analysing observables. Observables of a stochastic process are generally averaged values. The motivation for fBm was its power law behaviour of the MSD. Therefore, it is reasonable to analyse first the MSD. It can be calculated as a ensemble- or time-average. A difference in time- and ensemble-average would show a violation of ergodicity. A comparison of all four implemented algorithms can be seen in fig. 1.3. Here, $\Theta = \sqrt{2K_\alpha \Delta t^\alpha}$ is go-

1. Compute the auto-covariance function R_n^ξ of a periodic stochastic process ξ_n:

$$R_n^\xi = \begin{cases} K_\alpha \Delta t^\alpha \left[(n-1)^\alpha - 2n^\alpha + (n+1)^\alpha \right] & \text{for } 0 \leq n \leq M \\ R_{2M-n}^\xi & \text{for } M \leq n \leq 2M \end{cases}$$
(1.52)

2. Transform the auto-covariance function via FFT. The result is called the spectral density of the stochastic process ξ_n:

$$S_k^\xi = \text{FFT}(R_n^\xi; k)$$
(1.53)

3. Calculate $\tilde{\xi}_k$ the Fourier transform of the stochastic process ξ_n:

$$\tilde{\xi}_k = \begin{cases} \sqrt{2S_k^\xi M}(\eta_k) & \text{for } k = 0 \\ \sqrt{S_k^\xi M}(\eta_k + i\eta_k) & \text{for } 0 \leq k \leq M \\ \sqrt{2S_k^\xi M}(\eta_k) & \text{for } k = M \\ \tilde{\xi}_{2M-k}^* & \text{for } M \leq k \leq 2M \end{cases}$$
(1.54)

   $\{*\}$ denotes the complex conjugate, η_k is a random Gaussian variable with zero mean and variance 1 $[\eta_k \sim \mathcal{N}(0,1)]$.

4. Perform the inverse Fourier transform on $\tilde{\xi}_k$ and use the first half of the resulting stochastic process ξ_n:

$$\xi_n = \frac{1}{\sqrt{2M}} \text{FFT}^{-1}(\tilde{\xi}_k; n) \qquad \text{for} \quad 0 \leq n \leq N$$
(1.55)

5. perform the cumulative sum on the increments:

$$B_n^\alpha = \sum_{j=0}^n \xi_j \qquad \text{for} \quad 0 \leq n \leq M$$
(1.56)

Table 1.4: The table shows Davis-Harte fBm-generating algorithm [15].

ing to be the scale defining quantity in space. The MSD is displayed in units of Θ^2. MSDs for the algorithm are scaled with $k = 0.1, 1, 10, 100$ for Davis-Harte, Cholesky, Naive, Lowen, respectively, for a better visualisation. The theoretical scaled MSD $\delta r^2(t) = 2K_\alpha k t^\alpha$ are displayed as solid black lines. All algorithm show good accuracy between ensemble and time averaged MSD, besides for long lag times for the
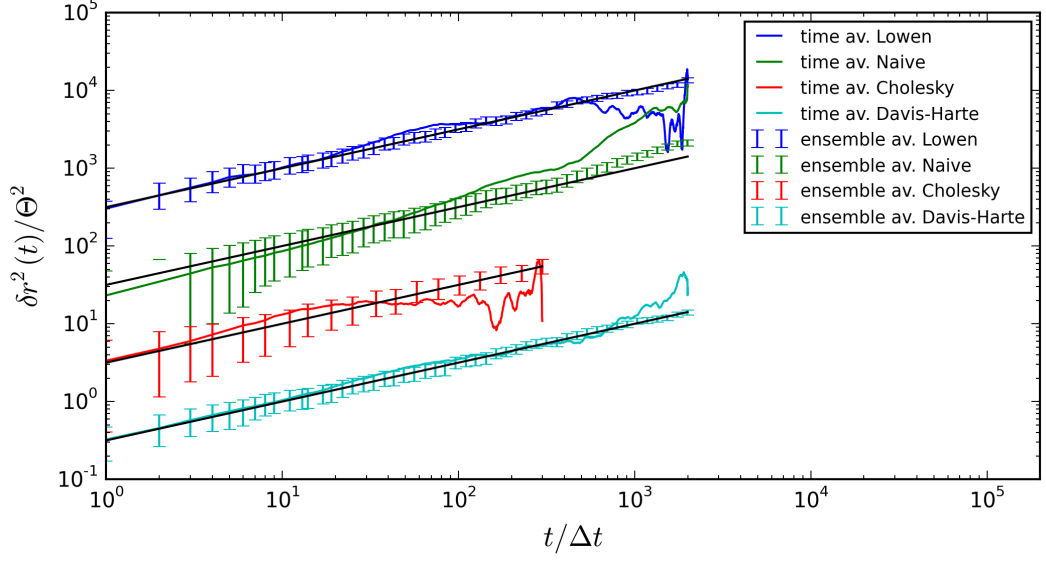
Figure 1.3: Comparison of MSD between time-average, ensemble-average over $N = 1000$ trajectories with trajectory length $M = 2000$ (Cholesky: $M = 300$) and $\alpha = 0.5$ for four algorithms. Cyan coloured line: Davis-Harte with $k = 0.1$, red coloured: Cholesky $k = 1$, green coloured: Naive $k = 10$, blue colour Lowen $k = 100$.
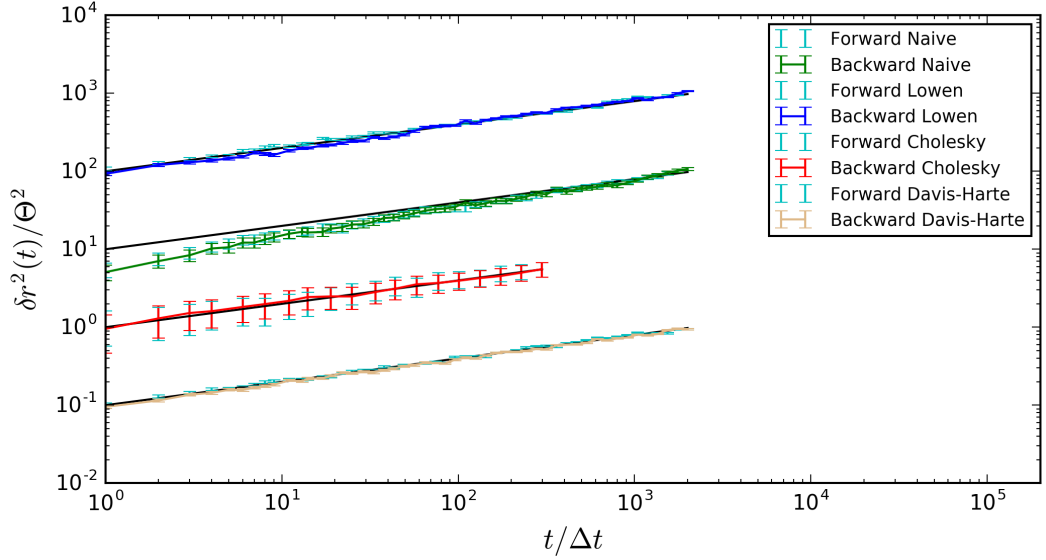

Figure 1.4: The plot show ensemble-averaged MSDs for forward time and backward time over $N = 2000$ (Cholesky: $M = 300$) trajectories with trajectory length $M = 1000$ $\alpha = 0.3$, brown coloured line: Davis-Harte with $k = 0.1$, red coloured: Cholesky $k = 1$, green coloured: Naive $k = 10$, blue colour Lowen $k = 100$. All backward trajectories are cyan coloured

time-averaged MSD due to decreasing statistics. The naive algorithm tends to result in too small MSDs for small lag times particularly for small α, which is going to be shown later on. This is caused by the finite number of samples in the discrete Fourier transform. In the following figures all MSD plots are ensemble averages.

Secondly, time-reversibility was checked. FBm is an equilibrium process and thus should be time reversible [19]. A time reversed trajectory can be defined as:

$$\overleftarrow{B}^{\alpha}_{n} = B^{\alpha}_{M} - \sum_{j=0}^{M} \xi_{M-j} \tag{1.57}$$

In fig. 1.4 MSDs of normal fBm and reversed-time fBm described by eq. (1.57) are plotted with the previously introduced scaling parameter k for better visualisation. No difference can be seen. Thus, all algorithm generate an equilibrium process. α had been chosen to be 0.3. Thereby the naive algorithm has an even stronger deviation from the desired power law because of the problem of the finite number of samples in the discrete Fourier transform. A strong influence of α on the accuracy of MSD for the naive algorithm is suspected. Hence, the influence of α on the MSD accuracy was studied next. The influence of α on the MSD for all four algorithms is shown in fig. 1.5. No deviations for Lowen, Cholesky and Davis-Harte can be seen. Cholesky and Davis-Harte algorithm work also in the range of $1 < \alpha < 2$. In the limit of Brownian motion ($\alpha = 1$), the artefacts of the naive algorithm vanish. Cholesky, Lowen and Davis-Harte show no deviation to the expected MSD for all α.

FBms property of self-similarity can be used to plot a scale-free version of the density distribution ($\mathcal{P}_{gauss}(\hat{r})$). The scale-free version was introduced in eq. (1.28). The scaled density distribution is not depended on time. Time rescaling leads to a "data collapse". In fig. 1.6 histograms over $N = 10000$ single trajectories at various times ($100 \leq t \leq 1000$) were calculated and rescaled according to eq. (1.28). The histograms were scaling for different algorithms with the scaling parameter k for better visualisation. For Cholesky and our algorithm no deviations from the theoretical values are obvious. For Lowen algorithm, systematically small changes to the theoretical value can be observed. However, the distribution of fBm should stay a Gaussian for all times. As introduced in eq. (1.31), the non-Gaussian parameter ($NGP(t)$) should be zero. The Non-Gaussian parameter was plotted for $0 \leq t \leq 1000 (\leq 356$ for Cholesky) and $\alpha = 0.5$ in the left fig. 1.7. The Naive, Davis-Harte and Cholesky algorithm perform as expected. Lowen however, shows deviations from a Gaussian distribution increasingly towards the end of the trajectory. In the right fig. 1.7, the influence of α on the non-Gaussian parameter for the Lowen algorithm was tested. For small α, the distribution is closer to a Gaussian. In our implementation, Lowen algorithm is not exact as claimed in [14]. A modification to the algorithm was introduced in the third point of the algorithm (see table 1.3). The modification introduces the correlation with random complex numbers generated in the rectangular representation, just like in Davis-Harte algorithm in its third point for $0 \leq k \leq M$. The resulting accuracy of MSD and a comparison of the non-Gaussian parameter for different α are shown in fig. 1.8. Modified
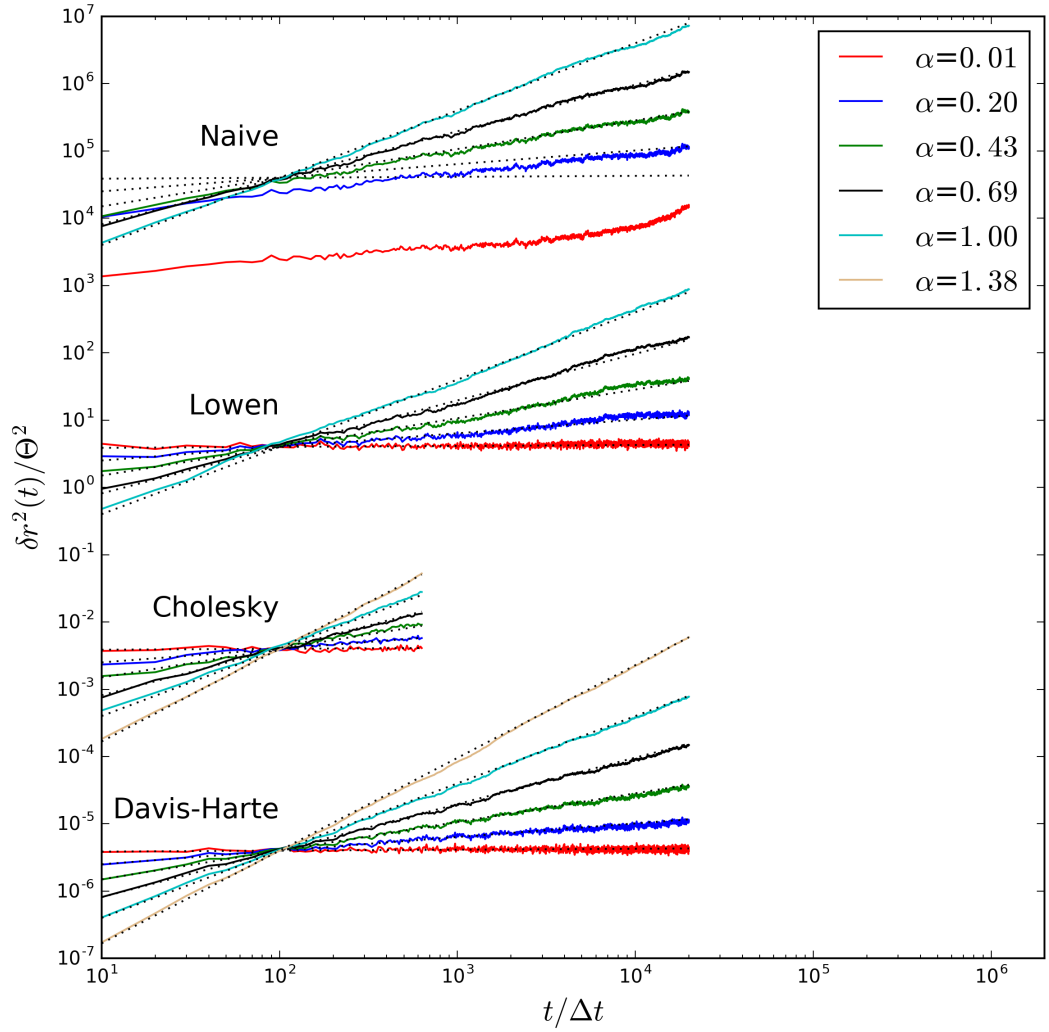
Figure 1.5: The figure shows ensemble-averaged MSDs for all four algorithms over $N = 400$ trajectories with the trajectory length $M = 2000$ (Cholesky: $M = 64$) and $0.01 \leq \alpha \leq 1.0$ (Cholesky and Davis-Harte $\alpha \leq 1.38$).

Lowen algorithm shows no deviation in the MSD and Non-Gaussian parameter to the desired theoretical values.
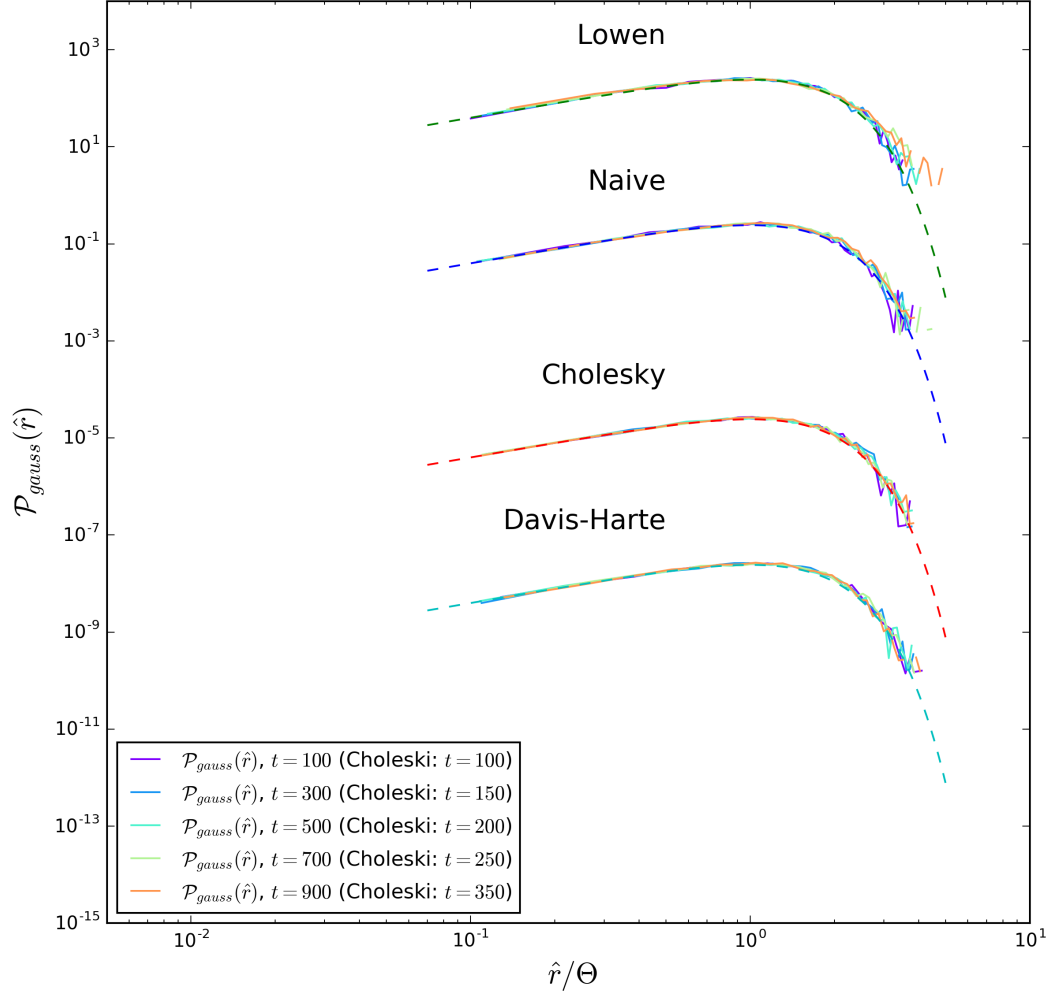
Figure 1.6: All four plots show the scale-free form of the propagator $\mathcal{P}_{gauss}(\hat{r})$ at different times as introduced in eq. (1.28) as an histogram over $N = 10000$ trajectories for $\alpha = 0.5$ at different times $100 < t < 900$. The dashed line show the expected distribution.

Performance Analysis

The performance with trajectory length and number of trajectories was analysed in figs. 1.9 and 1.10. Thereby, the very promising, in terms of exactness, Cholesky algorithm scales with $\mathcal{O}(M^3)$ with trajectory length M. Our application of an fBm-generating algorithm desires long trajectories. It is not reasonable to use such a slow algorithm. Even if every next trajectory with same α and length scales with $\mathcal{O}(M^2)$ [12]. Modified Lowen and Davis-Harte seem also to be exact. Both scale with $\mathcal{O}(Mlog(M))$ due to the FFT. Lowen algorithm is even faster because it directly generates fBm. Davis-Harte algorithm generates fGn. Davis-Harte looses some performance on the cumulative summation of the increments. The performance
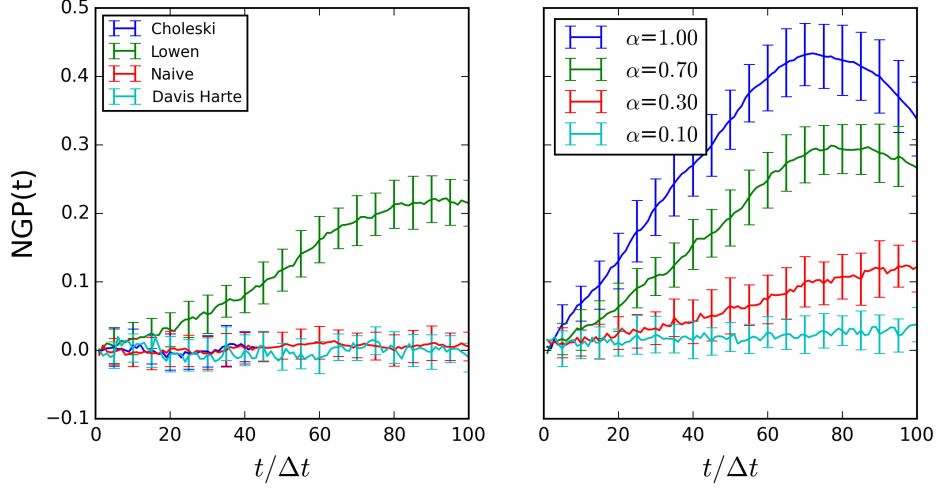
Figure 1.7: The left figure shows the Non-Gaussian-Parameter as introduced in eq. (1.31)
for all four algorithms with $N = 5000$, $M = 100$ and $\alpha = 0.5$ averaged over 30
non-Gaussian-Parameter with its variance displayed as an error-bar.
The right figure shows the Non-Gaussian-Parameter for Lowen algorithm with
$N = 5000$ and $M = 100$ for various $0.1 \leq \alpha \leq 1.0$ averaged over 30 non-
Gaussian-Parameter with its variance displayed as an error-bar.

with the number of trajectories is displayed in fig. 1.10. All algorithms scale linearly
with the number of trajectories N. Cholesky algorithm has an high offset but scales
then slowly with the number of trajectories . Although one should keep in mind,
that the trajectory length had to be chosen $M = 128$ compared to $M = 1000$ for
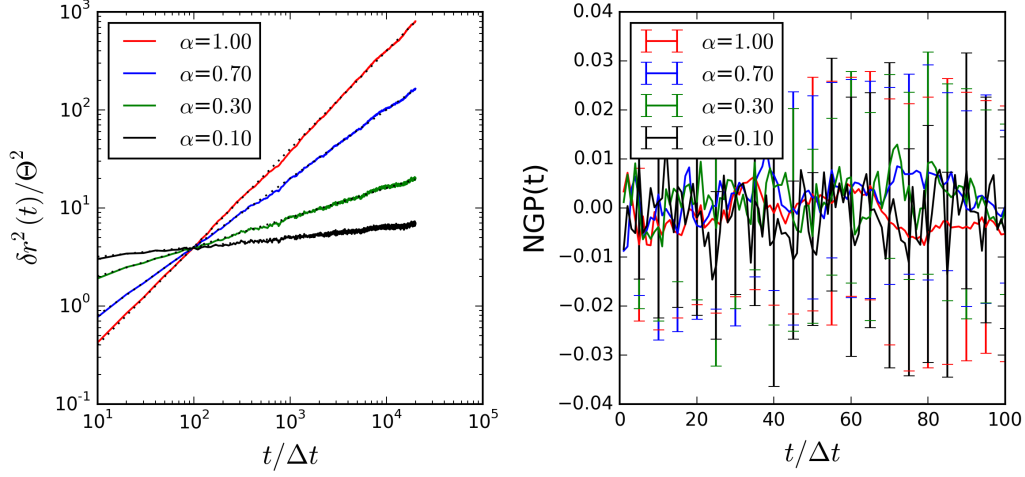the other algorithm to get comparably small values.

Figure 1.8: The left figure shows the MSD for various α in the range $0.1 \leq \alpha \leq 1.0$ generated by the modified Lowen algorithm with $M, N = 2000$.
The right figure shows the Non-Gaussian-Parameter for the modified Lowen algorithms with $N = 5000$, $M = 100$, $\Delta t = 0.1$ for various α in the range of $0.1 \leq \alpha \leq 1.0$ averaged over 30 non-Gaussian-Parameter with its variance displayed as an error-bar.
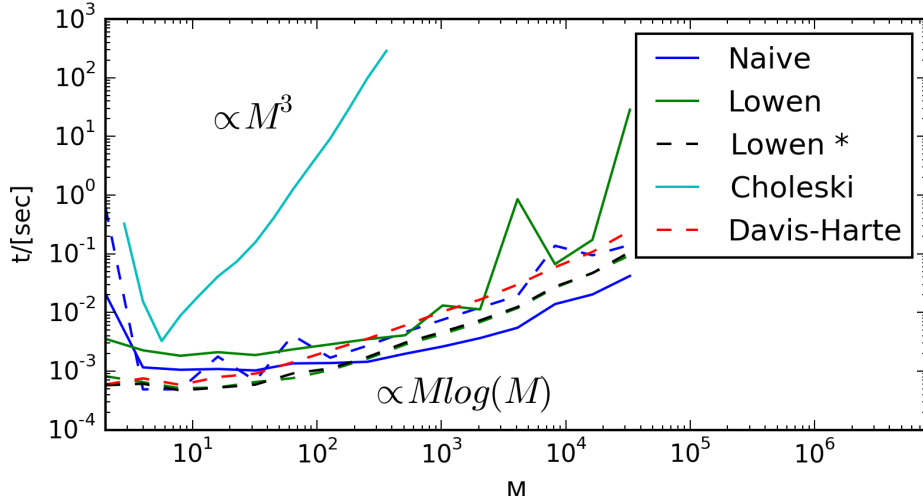
Figure 1.9: The algorithmic scaling of computational time with the trajectory length M for a single trajectory $N = 1$ is shown in the plot. Dashed lines are algorithms implemented in C++. Solid Lines are algorithms implemented in Python.
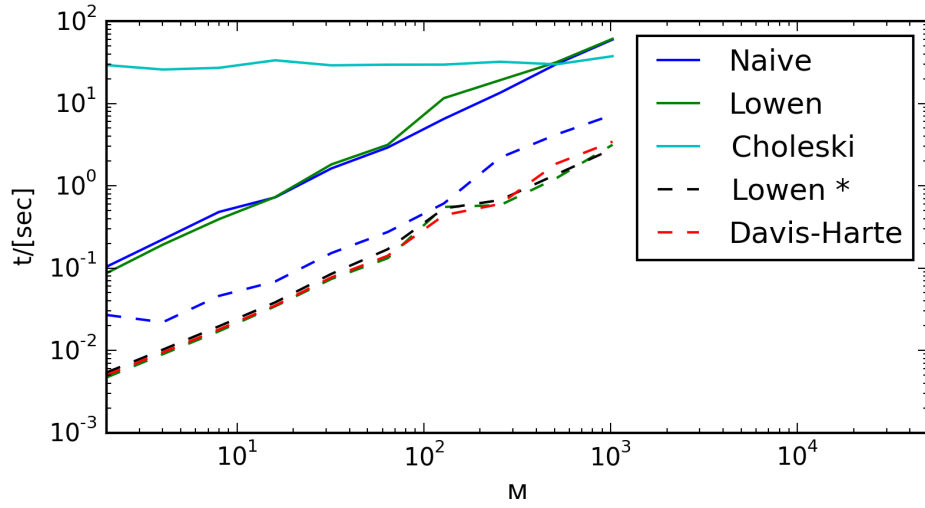
Figure 1.10: The algorithmic scaling of computational time with the number N of trajectories and trajectory length $M = 1000$ (Cholesky $M = 128$) is shown in the plot. Dashed lines are algorithms implemented in C++. Solid Lines are algorithms implemented in Python.

2 Particle Based Reaction Diffusion

Chemical reactions are ubiquitous in nature. They describe transformations of one or several chemical substances. Transformations of chemical substances are described by formation and breaking of chemical bonds. Physically precise, these bonds should be described quantum mechanically. Quantum mechanics is not needed for a description at cellular scales. Not to mention, that for such large systems these calculations cannot be performed. Hence, coarse-grained models for reactions at cellular scale were developed. But reactions in a broader sense can also be a transformations of one state to another one (e.g. protein changing its conformation). Biochemical reactions give rise to the complexity of life and are of key importance for processes in living cells. Indeed, Biochemistry is a whole area of research.

Early pioneer work on reactions, by Guldberg and Waage already in 1864 [20], resulted in the law of mass action, which states the proportionality of the reaction rate to the product of concentrations for elementary molecular reactions. Thereby, spatial resolution is neglected. The system is described in terms of a concentration (well-mixed assumption). The mass action law leads to a deterministic model described by ordinary differential equations (ODEs). Quantities like reaction kinetics and number of reactants in equilibrium can be obtained. Deterministic models, however, are not resolving stochastic phenomena. Stochastic models provide a more detailed understanding of the reaction-diffusion processes. Such a description is often necessary for the modelling of biological systems, where small molecular abundances of some chemical species make deterministic models inaccurate or even inapplicable [21]. Stochastic models based on the mass action law are characterised by the chemical master equation (CME). CME describes the temporal evolution of probabilities for the system to occupy each different state. The interesting topic of chemical kinetics described by CME will not be part of the elaborations. Nevertheless, for the sake of completeness, it was to be mentioned that stochastic simulations based on CME with the Gillispie algorithm [22] are performing very efficiently. Even spatial resolutions can be achieved with simulations based on the reaction-diffusion master equation (RDME [23]). Still, the well-mixed assumption has to hold at least for the compartments in the RDME model. A more detailed model is given by particle-based reaction-diffusion dynamics (PBRD)[24, 25]. Thereby, all particles are modelled as points or spheres and are resolved in space and time. However, the size of common biological systems surpasses computational feasibility. So further coarse graining gets necessary. Difficulties in simulations of biological systems arise on the one hand from very large systems and on the other from small molecular abundances of some chemical species. The well-mixed assumption does not hold. A less prominent approach is a PBRD model with fractional Brownian dynamics. Fractional Brownian motion approximates the motion of a particle in a crowded

biological medium. The motion of the media itself has not to be modelled explicitly. Therefore, PBRD simulations can be performed just for the relevant reacting particles. Stochastic particle-based models conventionally rely on Brownian or Langevin dynamics for the description of diffusion. Brownian dynamics was introduced in chapter 1. Langevin dynamics will not be examined explicitly. In short, it further includes the relaxation of particles momentum and reaches Brownian dynamics in the limit of strong damping, or at long time scales.

This chapter deals with some theoretical considerations on the impact of diffusion on reaction rates. The first section examines Smoluchwoski's pioneering work [26] on diffusion-limited reaction kinetics of a bi-molecular reaction and Erban/Chapmman extensions [27] for diffusion-influenced bi-molecular reactions. Thereby, a dependence of macroscopic reaction rates and the diffusion of the particles can be seen. These results shall motivate investigations of reaction-diffusion dynamics with a different diffusion model. Along the way the law of mass action is shown to follow under certain conditions from the diffusion eq. (1.5) motivated and introduced in the first chapter. These derivations further motivate both, models based on the law of mass action and PBRD models. RevReaDDy, a realisation of the latter, is then introduced and explained in the second section of this chapter.

2.1 Diffusion-Influenced Bi-molecular Reaction

Uni- and bi-molecular elementary reactions are most relevant in nature. According to collision theory, tri-molecular elementary reactions are negligible. Diffusion is not relevant for uni-molecular reactions. It is reasonable to start our considerations on how diffusion influences chemical reactions with the Smoluchowski problem for kinetics of a bi-molecular chemical reaction in solution. One particular area of research on which the Smoluchowski relation had a significant impact in the last few decades is biology. This is unsurprising as a vast number of biomolecular systems involve dilute and minute diffusing molecular populations undergoing continuous reaction. Understanding how these biological systems operate is complicated and is in itself a whole field of research; systems biology. The Smoluchowski result has provided a very powerful tool for theoretical investigation of microscopic biochemical reaction-diffusion processes [28]. It was extended by P. Debye in 1942 to add intermolecular forces. However, especially in biological systems Brownian motion do not apply for all time-scales. These environments exhibit very often anomalous diffusion, which can be addressed by fBm.

The following derivation shall give the kinetics of a simple model for a bi-molecular reaction and motivate a particle-based simulation scheme. The reaction scheme for a bi-molecular reaction with reactants A and B associate into a complex AB with a rate k_{d}^{+} and decay into A and B with a rate k_{d}^{-}. The chemical reaction can be written as:

$$\mathrm{A + B} \; \underset{k_{\mathrm{d}}^{-}}{\overset{k_{\mathrm{d}}^{+}}{\rightleftharpoons}} \; \mathrm{AB} \qquad\qquad (2.1)$$
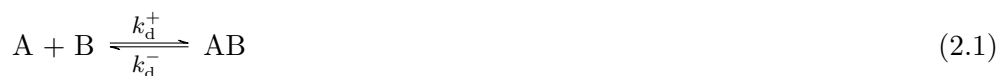
Free diffusion of particle A and B with the diffusion constants D_A and D_B, respectively, are assumed. Further no interactions between them are present. In fact, this problem can be described by a modified version of the diffusion eq. (1.5) motivated in the first chapter. The joint concentration field $\rho_t(\boldsymbol{r}_A, \boldsymbol{r}_B)$ for a bi-molecular system in a solution obeys:

$$\frac{\partial \rho_t(\boldsymbol{r}_A, \boldsymbol{r}_B)}{\partial t} = (D_A \nabla_A^2 + D_B \nabla_B^2) \rho_t(\boldsymbol{r}_A, \boldsymbol{r}_B) \tag{2.2}$$

The complexity of the problem can be reduced by substituting the positions of the particles A and B with their relative distance $\boldsymbol{r} = \boldsymbol{r}_A - \boldsymbol{r}_B$. It is convenient to introduce even further substitutions:

$$D = D_A + D_B \qquad\qquad \boldsymbol{R} = \frac{D_B \boldsymbol{r}_A + D_A \boldsymbol{r}_B}{D_A + D_B} \tag{2.3}$$

the Laplace operator in terms of new coordinates result in:

$$\nabla_A^2 = \left(\nabla_r + \frac{D_B}{D} \nabla_R \right)^2 \tag{2.4}$$

$$\nabla_B^2 = \left(\nabla_r + \frac{D_A}{D} \nabla_R \right)^2 \tag{2.5}$$

By inserting eq. (2.4) and (2.5) in eq. (2.2) the following result can be obtained:

$$\frac{\partial \tilde{\rho}_t(\boldsymbol{r}, \boldsymbol{R})}{\partial t} = \left(D \nabla_r^2 + \frac{D_B D_A}{D_A + D_B} \nabla_R^2 \right) \tilde{\rho}_t(\boldsymbol{r}, \boldsymbol{R}) \tag{2.6}$$

This equation describes two independent diffusion processes, one in the coordinate $\boldsymbol{r}$ and one in the coordinate $\boldsymbol{R}$. The solution can be obtained by the product ansatz $\tilde{\rho}_t(\boldsymbol{r}, \boldsymbol{R}) = \rho_t(\boldsymbol{r}) q_t(\boldsymbol{R})$. Integration over $\boldsymbol{R}$ results in:

$$\frac{\partial \tilde{\rho}_t(\boldsymbol{r}, \boldsymbol{R})}{\partial t} = D \nabla_r^2 \rho_t(\boldsymbol{r}) + \frac{D_B D_A}{D_A + D_B} \int_{\partial V} \nabla_R q_t(\boldsymbol{R}) d\boldsymbol{a} \tag{2.7}$$

In the previous equation the stokes theorem was applied. The integral in the second term is zero due to conservation of probability. The problem is isotropic, hence $r = |\boldsymbol{r}|$ and $\nabla_r^2 = \left(\partial_r + \frac{2}{r} \right) \partial_r$. The equation reduces to the one-dimension form of the continuity eq. (1.6) without any production term:

$$\frac{\partial \rho_t(r)}{\partial t} = -\left(\frac{\partial}{\partial_r} + \frac{2}{r} \right) j_t(r) \qquad\qquad j_t(r) = D \frac{\partial \rho_t(r)}{\partial_r} \tag{2.8}$$

The stationary distribution satisfies:

$$-\left(\frac{\partial}{\partial_r} + \frac{2}{r}\right) j^s(r) = 0 \tag{2.9}$$

$$\frac{dj^s(r)}{j^s} = -\frac{2}{r} dr \tag{2.10}$$

$$j^s(r) = Ar^{-2} \tag{2.11}$$

$$\rho^s(r) = \rho^s(\sigma) - \frac{\int_\sigma^r j^s(r')dr'}{D} = \rho^s(\sigma) + \frac{A}{D}\left(\frac{1}{r} - \frac{1}{\sigma}\right) \tag{2.12}$$

Here, σ is defining a distance between particle A and B. It is going to be the scale defining quantity in space. For particles A and B closer than σ instantaneous reactions occur and the joint concentration equals zero ($r \leq \sigma \Rightarrow \rho_t(r \leq \sigma) = 0$). Now, let's assume only a single molecule B being at the position $r = 0$ and a constant concentration of particles A at infinity ($\rho_t(r \to \infty) = c_A$). The frame of reference is the B particle. This approximation, where the distribution of particle A around a single particle B is studied without any B particles, besides the one in the origin, should also be true for a low concentrations of B particles relative to A particles ($c_B \gg c_A$). Two or more B particles in proximity would disturb the concentration profile. The solutions for $\rho^s(r)$ and $j_t^s(r)$ for the upper boundary conditions are:

$$\rho^s(r) = c_A\left(1 - \frac{\sigma}{r}\right) \qquad j^s(r) = -D\sigma c_A r^{-2} \tag{2.13}$$

With eq. (2.1) in mind it should be clear, that the production of c_{AB} originates from the flux of particles at σ. The production of the concentration of c_{AB} is then:

$$\frac{dc_{AB}}{dt} = 4\pi\sigma D c_A c_B \tag{2.14}$$

Along the way several assumptions were made:

- The system can be described by a diffusion constant which is independent of the time and and position.

- No interaction between particles are present (ideal gas).

- The system has a constant background concentration of A particles $\rho_t(r \to \infty) = c_A$.

- The dynamics are stationary.

- The reaction is limited by diffusion. Since, reactions occur instantaneously at $r = \sigma$.

Still, the solution gives the kinetics for a simple bi-molecular system. It is consistent with collision theory, which states that the collision frequency is proportional to the concentrations of the colliding particles. Pioneer work on reaction kinetics by Guldberg and Waage already in 1864 [20] resulted in the law of mass action which

states for elementary uni- and bi-molecular reactions, the proportionality of the reaction rate (r_f) to the concentration.

$$r_f = k_f c_A c_B \tag{2.15}$$

This equation provides the basis for a description of reaction kinetics in terms of ordinary differential equations (ODEs) like eq. (2.14).

Smoluchowski's problem can be, in fact, generalised for reactions to occur with a finite microscopic rate λ_+ within a radius σ, derived by Erban and Chapman [27]. However, as a small remark, the microscopic rate has to be distinguished from the macroscopic rate. As an example microscopic rates are related to the Kramers problem, describing the time dependence of a particle passing a potential barrier e. g. commonly in biology protein binding / unbinding. The generalized problem can be described similarly to Smoluchwoski's problem eq. (2.8) with an production term continuity eq. (1.6) :

$$\frac{\partial}{\partial t} c(\boldsymbol{r}, t)) = -\nabla J(\boldsymbol{r}, t) - \lambda_+ c(\boldsymbol{r}, t) \mathrm{H}(\sigma) \tag{2.16}$$

Here, $\mathrm{H}(\sigma)$ is the Heaviside step function. The derivation of a stationary solution of the second-order ODEs analogously to the Smoluchowiski problem can be found in the appendix 5.4. The solution shows again the possibility of describing the production with a macroscopic reaction rate $k_+(\kappa, \sigma)$:

$$k_+ = 4\pi D\sigma \left(1 - \frac{1}{\sigma\kappa} \tanh \sigma\kappa\right) \tag{2.17}$$

Here, $\kappa = \sqrt{\lambda_+/D}$ and $1/\kappa$ can be intuitively interpreted as the penetration length of A particles into the shell with distance σ around B particles. The scenario in two dimensions is visualised in fig. 2.2. The law of mass (eq. (2.15)) still holds for a bi-molecular reaction not only in the diffusion limit. but also for reactions occurring with a certain microscopic rate, under the well-mixed assumption and normal diffusion. ODEs for the system can be formulated. There solutions give the kinetics and concentrations in equilibrium, but no information on the spatial distribution are contained.

For the generalised problem with a microscopic rate λ_+, a diffusion- and microscopic reaction-limit can be shown. For $\lambda_+ \to \infty$ reactions occur immediately and the diffusion-limit is reached. If $\lambda_+ \ll D/\sigma^2$ a Taylor expansion of the Tangens Hyperbolicus in eq. (2.17) is given by:

$$\tanh x \to 0 \approx x - \frac{x^3}{3} \tag{2.18}$$

and eq. (2.17) can be approximated as:

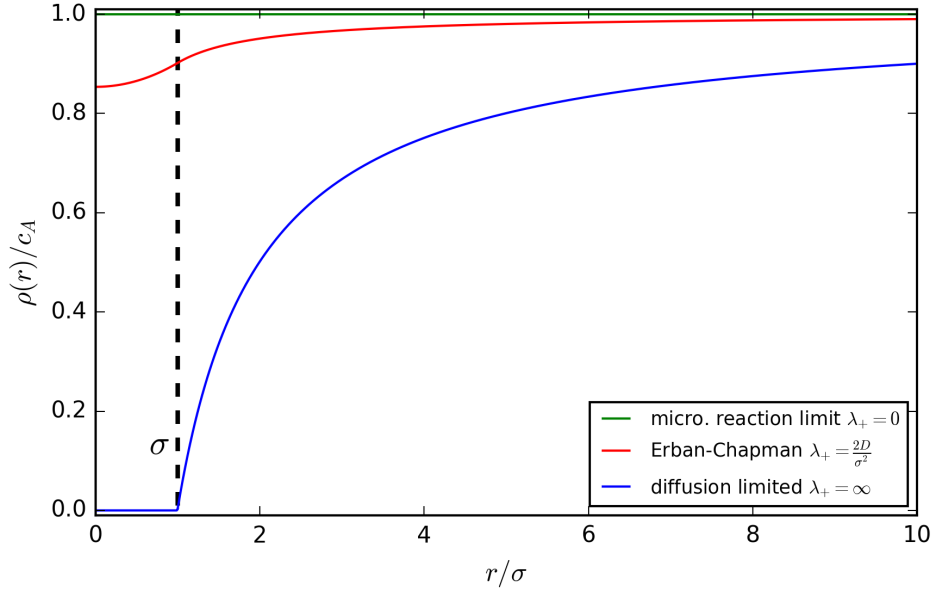$$k_+ = \frac{4\pi\sigma^3 \lambda_+}{3} \tag{2.19}$$

Figure 2.1: Density distribution from eqs. (5.19) and (5.20) for a bi-molecular reaction from the Erban-Chapman derivation for three scenarios:

1. The microscopic reaction limit for $\lambda_+ = 0.0$ displayed as a green solid line

2. An intermediate scenario with $\lambda_+ = 2d/\sigma^2$ displayed as a blue solid line.

3. Smoluchwski's result for diffusion-limited reactions $\lambda_+ = \infty$.

The macroscopic reaction rate no longer depends on diffusion but solely on the microscopic reaction rate. The stationary distributions for both limits and an intermediate scenario are plotted in fig. 2.1.

The previous elaborations show that macroscopic reaction rates dependent on diffusion for bi-molecular reactions. For simple reaction-diffusion systems the evolution and the stationary distribution of the density distribution can be obtained by solving Smoluchwoski's equation (PDE). For the bi-molecular reaction the law of mass action could be seen to follow for spatial homogeneity. Then reaction kinetics can be described for easy systems in terms of ODEs. Nevertheless, for complex systems often no closed solution is known. Further, for small molecular abundances of some chemical species deterministic models get inaccurate or even inapplicable. Stochastic models are necessary. Via chemical master equations (CMEs) and reaction-diffusion master equations (RDMEs) analytical stochastic results can be obtained. Deduced from the Master equation also stochastic simulations based on Monte Carlo methods, like the prominent Gillispie algorithm [22], can be performed. This chapter, however, aims to introduce PBRD. The implementation of a PBRD simulation introduced in the next section follows the theoretical description of reactions with microscopic reaction rates within a reaction radius in this section.

2.2 RevReaddy with fBm

RevReaDDy is a PBRD tool developed by Christoph Fröhner within his PhD project under supervision of Frank Noé. It is not published. Many modification to the tool had to be done in the process of this thesis. ReRreaDDy is based on the simulation package ReaDDy by Johannes Schöneberg and Frank Noé [29]. Reaction-diffusion dynamics of all particles can be resolved in space and time. Particles are modelled as spheres with possible particle interaction potentials. The tool aims to bridge the gap between molecular simulation and CME/RDME simulations. It is written in C++. However, the user can setup up and simulate the desired reaction scheme in Python via a Python binding. Particle types with a specific radius and diffusion constant can be defined. Particles of a predefined particle type can be placed anywhere into a simulation box with variable box size and periodic boundary conditions. A desired simulation length and width of the time step have to be set. Conventionally particles propagate by Brownian Dynamics. In the process of the thesis also a fractional Brownian motion integrator with the circulant method by Davis-Harte [12] and Lowen [14] was implemented. For Brownian Dynamics, potentials with two different potential types, Lennard Jones and soft repulsion, can be introduced to act in-between particles and between fixed geometries in the simulation box and particles. Thereby, a temperature has to by defined. Particles can be e.g limited to diffuse on a surface by a potential. It can be chosen from various reaction types to affect the particle types. For uni-molecular reactions like conversion $A \underset{k'}{\overset{k}{\rightleftharpoons}}$ B, annihilation $A \xrightarrow{k} \emptyset$, decay $A \xrightarrow{k} B + C$ the probability that one particle undergoes a reaction within the timestep (Δt) is simply approximated as:

$$P(n) = 1 - \exp[-\lambda \Delta t n] \approx \lambda \Delta t n \qquad \text{for} \qquad P(1) \ll 1 \tag{2.20}$$

Here, $n = t/\Delta t$. A more sophisticated algorithm, which draws the reaction time from the correct distribution is the Gillispie algorithm [22]. It could by implemented into RevReaDDy as an improvement. For such reactions, microscopic reaction rates λ are independent of the position.

For a decay reaction a weighting factor and reaction distance shall be defined. They determine how far each of the particles are placed from the previously existing complex. With the waiting factor equals zero, particle A is placed at the position of the pre-existing complex and particle B is placed with a uniform distribution in the sphere with reaction radius σ. For bi-molecular reactions like the enzymatic reaction with complex building $A + B \underset{k'}{\overset{k}{\rightleftharpoons}} A + C$ or fusion $A + B \xrightarrow{k}$ C relative positions of the reactants are important for the reaction to take place. Analogous to the setup up of Erban and Chapman in section 2.1 a microscopic reaction rate λ within a reaction distance σ have to be defined. If the reactants come closer than σ a reaction takes place with probability $P = \lambda \Delta t$ during Δt. The problem is visualised in fig. 2.2. Thereby the time step cannot by chosen arbitrarily large. The mean square displacement for Brownian motion in three-dimensions is given as $\delta r^2(\Delta t) = 6D\Delta t$. The mean displacement during one time step has to
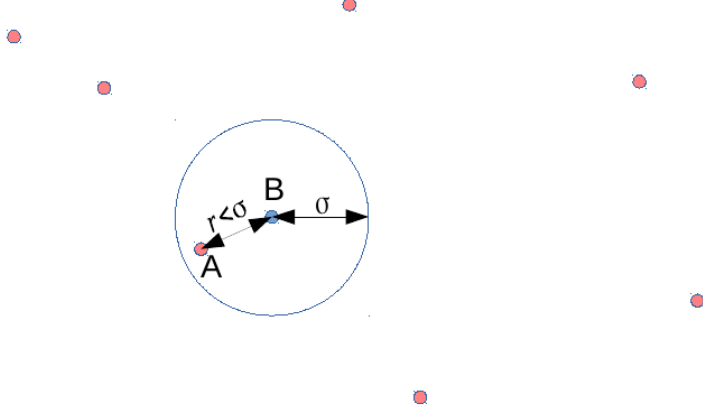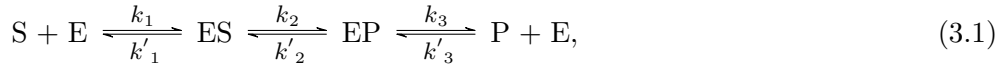
Figure 2.2: The Figure shows a visualisation of a bi-molecular reaction between particle A and B in RevReaDDy. Particle B are coloured blue and particle A are coloured red.

be a lot smaller than the squared penetration length $\delta r^2(\Delta t) \ll 1/\kappa^2$. Otherwise differences between the time of particles staying within a radius σ to another particle would differ significantly in comparison to $\Delta t \rightarrow 0$. Thus, also the macroscopic reaction rates would become less accurate. For fractional Brownian motion with $\alpha < 1$ the effect increases. A variety of observables are provided in RevReaddy, which are written into HDF5 files [30] during the simulation. Possible observables are: Acceptance rate, energy, mean square displacement, particle number, radial distribution functions, number of reactions, increments and positions. Observables can mostly be defined to consider any particle type over any period in time.

3 An Enzymatic Reaction With Fractional Brownian Motion

The biochemical reactions taking place in cells, though thermodynamically favourable, are in most cases very slow if left uncatalysed. For example, the spontaneous cleavage of a peptide bond would take 400 years at room temperature and phosphomonoester hydrolysis, routinely breaking up ATP to release energy, would take about a million years in the absence of the enzymes that shuttle that reaction along [31]. They have a defined amino acid sequence and a three-dimensional structure. The specific three-dimensional structure contains an active site for a substrate molecule to bind and orient and a catalytic site to reduce the chemical activation energy. Usually, an enzyme molecule has only one active site, and the active site fits with one specific type of substrate. So enzymes mostly have a high specificity for a particular type of reaction. After reaction takes place the product is released. The enzyme is free to start the reaction circle with a new substrate. Many reversible intermediate states can be present in the reaction mechanism. A simple representation of the mechanism with two complex intermediate states can be written as:

$$\text{S} + \text{E} \underset{k'_1}{\overset{k_1}{\rightleftharpoons}} \text{ES} \underset{k'_2}{\overset{k_2}{\rightleftharpoons}} \text{EP} \underset{k'_3}{\overset{k_3}{\rightleftharpoons}} \text{P} + \text{E}, \tag{3.1}$$

Here, k are the forward rates and k' the backward rates. S and P are substrates and products, respectively. ES and EP are intermediate complexes. By the law of mass action, ODEs can be formulated but often no closed solution exists.

The focus of this chapter is to study the kinetics and spatial distribution of the Michaelis-Menten mechanism, an even simpler mechanism, in the presence of normal and fractional Brownian motion. Monte Carlo simulations with anomalous diffusion modelled by a random walk between immobile obstacles were performed by Berry [32], Schnell and Turner [33]. An overview on stochastic modelling of in vivo reactions was given by Turner [34]. Recently, first passage time simulations with fBm were performed by Jeon *et al.* [35]. A Michaelis-Menten mechanism with fractional Brownian motion has not been studied yet.

3.1 Michaelis-Menten (MM) kinetics

Leonor Michaelis and Maud Menten proposed in 1913 a mathematical model for enzyme kinetics. Their most important contribution was to assume an enzyme-substrate to be present [4]. In their honour, it is also called Michaelis-Menten complex. A simpler version of eq. (3.1) was proposed as the Michaelis-Menten

mechanism:

$$S + E \xrightleftharpoons[k_-]{k_+} ES \xrightarrow{k_c} P + E \tag{3.2}$$

The backward reaction rate, from products and enzymes to complexes, was assumed to be negligible. They postulated the relation between the reaction velocity, formation of products, and the concentration of substrates. This relation is captured by the so called Michaelis-Menten equation:

$$v = \frac{v_{max}c_s}{K_M + c_s} \tag{3.3}$$

Here, v_{max} is the maximum reaction velocity. The Michaelis constant (K_M) is the substrate concentration with 50% of maximum velocity and (c_S) is the concentration of the substrate. A derivation of the Michaelis-Menten equation was done by Briggs and Haldane [36] in 1925, assuming the mass action law, mass conservation and a quasi-steady state approximation (QSSA). It states that after a negligible initial transition regime $(t \ll t_c)$ the concentration of the complex varies slowly as if in a quasi-steady state $(dc_{ES}/dt = 0)$. A set of differential equations can be formulated as a result of mass conservation and the mass action law:

$$\frac{dc_S(t)}{dt} = k_-c_{ES}(t) - k_+c_E(t)c_S(t), \tag{3.4}$$

$$\frac{dc_{ES}(t)}{dt} = -k_c c_{ES}(t) - k_-c_{ES}(t) + k_+c_E(t)c_S(t), \tag{3.5}$$

$$\frac{dc_P(t)}{dt} = k_c c_{ES}(t), \tag{3.6}$$

$$\frac{dc_E(t)}{dt} = k_c c_{ES}(t) + k_-c_{ES}(t) - k_-c_E(t)c_S(t), \tag{3.7}$$

with a quasi-steady-state approximation, one can reduce eq. (3.5) to: $k_+c_E(t)c_S(t) = k_-c_{ES} + k_c c_{ES}(t)$. A Rearrangement of this equation results in the Michaelis-Menten constant:

$$K_M = \frac{k_- + k_c}{k_+} = \frac{c_E(t)c_S(t)}{c_{ES}}. \tag{3.8}$$

The mass conservation law yields: $c_E(t) = c_{E_0} - c_{ES}(t)$. After inserting this equation into eq. (3.5), one obtains:

$$c_{ES}(t) = \frac{c_{E_0}c_S(t)}{K_M + c_S(t)} \tag{3.9}$$

The combination of this eq. with the differential eq. (3.6) defines the velocity of the reaction:

$$v(t) = \frac{dc_P(t)}{dt} = k_c \frac{c_{E_0}c_S(t)}{K_M + c_S(t)} = v_{max}\frac{c_S(t)}{K_M + c_S(t)} \tag{3.10}$$

where, $v_{max} = k_c c_{E_0}$ is the maximum velocity. In 1987 the approximation was shown to hold for $c_{E_0} \ll K_M$ or $K_M \ll c_{S_0}$ by Palsson [37]. In 1997 a closed form for the kinetics of the Michaelis-Menten mechanism with the quasi-steady state approximation was derived by Schnell and Mendoza [38]:

$$c_S(t) = K_M W_0 \left[\frac{c_{S_0}}{K_M} \exp \left(\frac{-v_{max}t + c_{S_0}}{K_M} \right) \right], \tag{3.11}$$

$$c_{ES}(t) = \frac{c_{E_0} c_S(t)}{K_M + c_S(t)} \{ 1 - \exp \left(- [K_M + c_S(t)k_+] \right) \}, \tag{3.12}$$

$$c_E(t) = c_{E_0}(t) - c_{ES}(t), \tag{3.13}$$

$$c_P(t) = c_{S_0} - c_S(t) + c_{ES}(t), \tag{3.14}$$

where, $W_0(x)$ is the upper branch of the Lambert W function. The quasi-steady state approximation was applied in the derivation of $c_S(t)$. A time independent concentration of complexes c_{ES} is conventionally solved for the transitions regime $t \ll t_c$ by approximating $c_S(t \ll t_c) \approx c_{S_0}$. For eq. (3.12), the result for the time independent c_{ES} was extended to the total time period $(0 < t < \infty)$ by applying time dependent $c_S(t)$ from eq. (3.11). For normal diffusion, these equation will be used to model the concentrations obtained from the simulation. Still, for a small number of particles the deterministic approach may differ from the averages of the stochastic simulation [34].

The quasi-equilibrium approximation is the second very common approximation, typically applied on setups with high enzyme concentrations. It is assumed that the binding step quickly reaches an equilibrium state $(c_S c_E/c_{ES} = K_S)$. $K_S = k_-/k_+$ is the dissociation constant and the rate of product formation can be written as:

$$v = \frac{V_{max} c_S}{K_S + c_S} \tag{3.15}$$

The assumption was shown to be true for $c_{E_0} \gg K_M$ or $k_- \gg k_c$ by Palsson [37].

An early description of reaction kinetics with fractional diffusion was done by Kopelman [39] for a percolation cluster with a scaling theory and an upgraded time depended reaction rates. This concept was applied by Berry [32] and Schnell [33] for the Michaelis-Menten mechanism.

3.2 Simulation Model

The simulation of the Michaelis-Menten mechanism eq. (3.2) and fractional Brownian motion with the circulant method by Davis-Harte [12] and modified Lowen was setup up with RevReaDDy. Four particle types were defined: substrate, product, complex and enzyme. The reaction radius σ will be used as units of length and Γ as units of time, with $\Gamma^\alpha = \sigma^2/6K_\alpha$. Substrates and products were set to diffuse with the same diffusion constant $K_\alpha = 1\sigma^2/\Gamma^\alpha$. Enzymes and complexes are modelled to be immobile with $K_\alpha = 0\sigma^2/\Gamma^\alpha$. Enzymes are typically larger than substrates or products and diffuse therefore slower $(D \approx k_B T/6\pi\eta a)$. A single enzyme was set in

the origin $(x, y) = (0, 0)$ and 20 substrates were placed randomly in the simulation box with periodic boundary conditions. The length of the quadratic box $L = 8\sigma$ was set fixed, but could be used as a parameter to control the concentration. Two association/decay reaction types were defined: S + E $\xrightleftharpoons[k_-]{k_+}$ ES and P + E $\xleftarrow{k_\mathrm{c}}$ ES with intrinsic reaction rates λ_+, λ_- and λ_c for complex formation, decay into substrate and enzyme and decay into product and enzyme, respectively. The reaction radius σ was set equal for both reaction types to 1σ. It defines the unit of length. A desired simulation length of $M = 2^{14}$ steps with a time step of width $\Delta t = 0.05\sigma^{2/\alpha}/6K_\alpha^\alpha\Gamma$ was set. In this simulation setup and regardless of α the particles on average travel for $n = 20$ steps to overcome the distance σ. Further the reaction probability as approximated in eq. (2.20) should be a lot smaller than $P(\Delta t) = \lambda\Delta t \ll 1$. Otherwise that approximations fails to describe the correct reaction probability $P(t) = 1 - \exp(-\lambda t)$. This is a short-coming of the implementation. Simulations for various λ_+, λ_-, λ_c and α were performed. The results are discussed in the next two sections.

3.3 Results for Normal Diffusion

First, simulations with normal diffusion were set up to validate our simulation model with the results from Smoluchowski [10] and Erban-Chapman [27] and classical Michaelis-Menten mechanism. The difference in kinetics of the Michaelis-Menten mechanism to the Erban-Chapman problem is a possible blocking of enzymes. Thus, slowing down the reaction speed. Also, a higher local concentration of substrates in close proximity to the enzyme is present because of the back reaction. At first, a reaction similar to the Erban-Chapman problem was aimed to simulate. Therefore, $\lambda_- = 0$ was chosen to avoid the effect of a higher local concentration of substrates and $\lambda_+ < \lambda_c$ to reduce enzyme blocking. Thereafter, the normal MM mechanism was studied.

3.3.1 One-Way Reactions

The first scenario will be referred to as the one-way "Erban-Chapman" reaction. It was performed under normal diffusion $\alpha = 1$ and with $\lambda_- = 0$, $\lambda_+ = 0.1/\Gamma$, $\lambda_c = 1.0/\Gamma$. The initial concentrations are $c_{S_0} = 5/128\sigma^3$ and $c_{E_0} = 1/512\sigma^3$. The reaction mechanism results in:

$$ \text{S + E} \xrightarrow{k_+} \text{ES} \xrightarrow{k_c} \text{P + E} \tag{3.16} $$
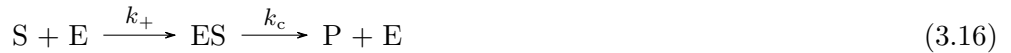
λ_+ was set to be the rate limiting step in the reaction chain and λ_c was set to reproduce approximately the Erban-Chapman problem. The normalised number of substrates $c_S(t)/c_{S_0}$, the normalised number of products $c_P(t)/c_{S_0}$ and the number of complexes $c_{ES}(t)$ was sampled over 2544 runs. The averages are visualised in a double logarithmic plot in fig. 3.1. Every run started with a new uniformly-distributed initial position of the substrate molecules in the simulation volume. The
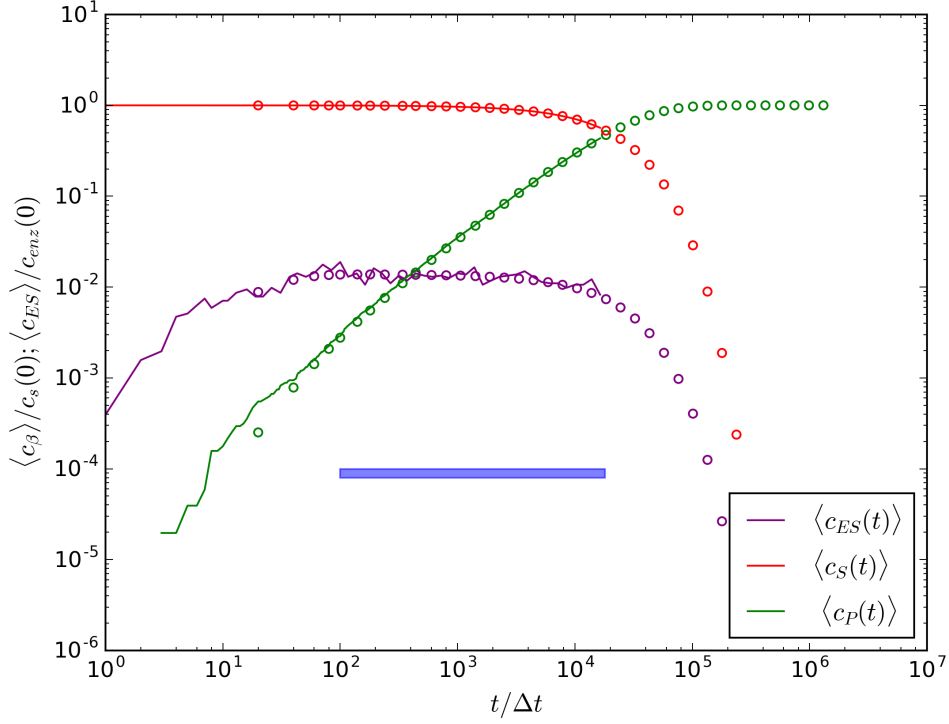
Figure 3.1: Scenario: The one-way "Erban-Chapman" reaction with microscopic reaction rates set to $\lambda_+ = 0.1/\Gamma$, $\lambda_- = 0$, $\lambda_c = 1.0/\Gamma$ is shown. Normalised concentrations of substrate, product and complexes are displayed as solid lines. eq. (3.11)(QSSA) was fitted to $c_s(t)$. The resulting $k_+ = 0.36\sigma^3/\Gamma$ from the fit was inserted in eqs. (3.12) and (3.14) and plotted as empty circles. The blue bar in the plot indicates the area where the radial distribution was sampled (see fig. 3.2). P
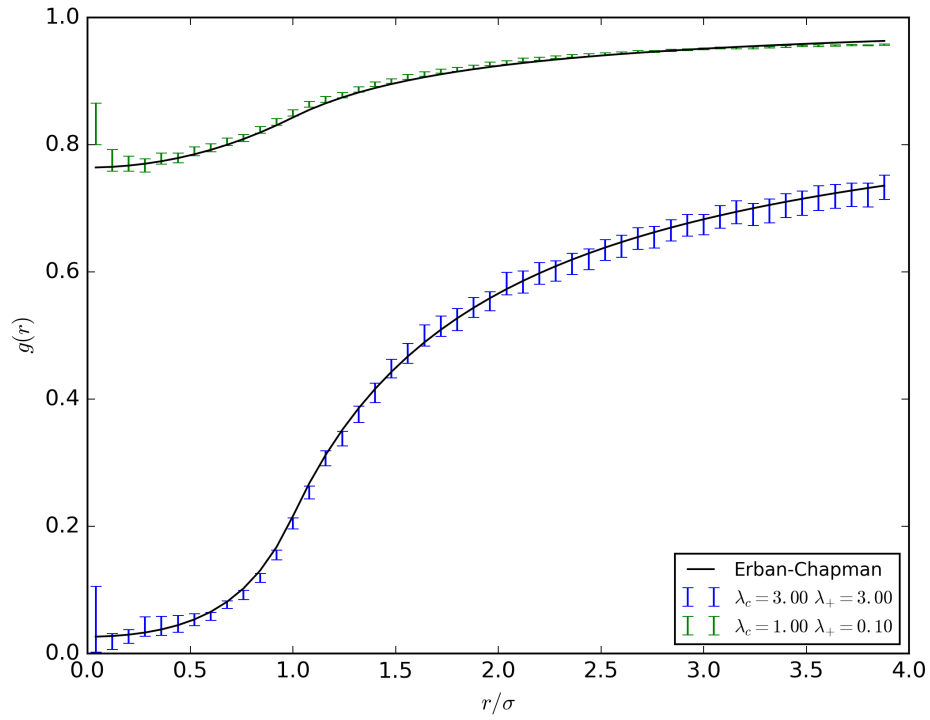
Figure 3.2: The radial distribution function 3.18 of the substrates around the enzyme/complex was sampled in the range of $(100\Delta t < t < 2^{14}\Delta t)$ and plotted as error-bars with the width of the standard deviation. The Erban-Chapman 5.19 result was plotted as a solid black line.
green: One-way "Erban-Chapman" reaction: $\lambda_+ = 0.1/\Gamma$, $\lambda_- = 0$, $\lambda_c = 1.0/\Gamma$.
blue: One-way "diffusion-limited" reaction: $\lambda_+ = 3.0/\Gamma$, $\lambda_- = 0$, $\lambda_c = 3.0/\Gamma$
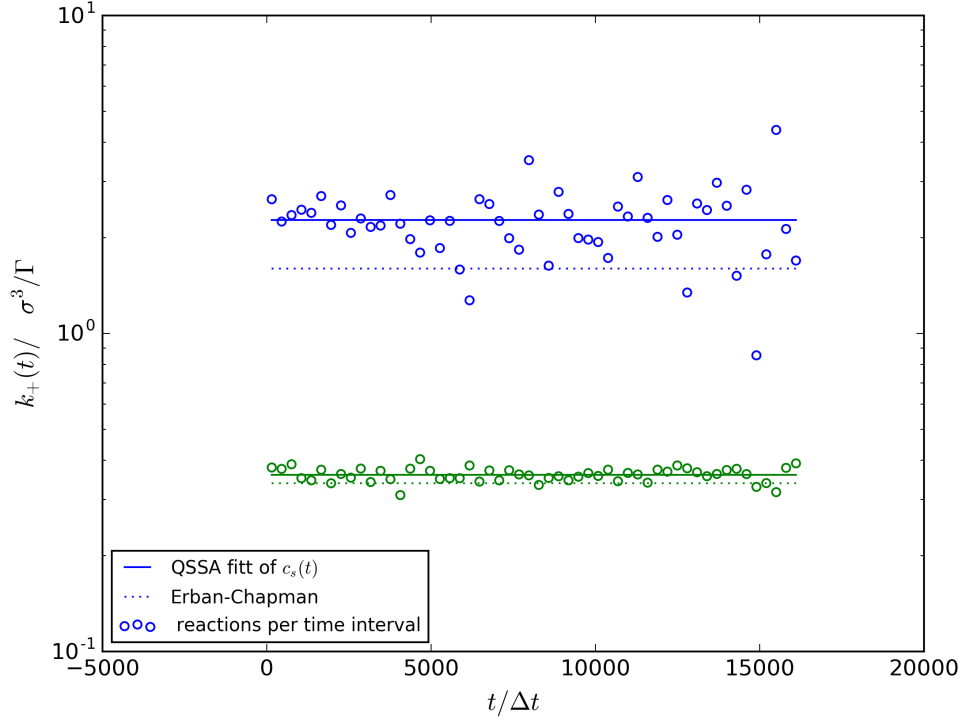
Figure 3.3: Two scenarios, with three different calculations of k_+ are displayed:

- green: One-way "Erban-Chapman" reaction : $\lambda_+ = 0.1/\Gamma$, $\lambda_- = 0$, $\lambda_c = 1.0/\Gamma$.

- blue: One-way "diffusion-limited" reaction: $\lambda_+ = 3.0/\Gamma$, $\lambda_- = 0$, $\lambda_c = 3.0/\Gamma$.

1. k_+^{QSSA} was calculated from the fit of the substrate concentration eq. (3.11) with the QSSA and displayed as a solid line

2. k_+^{count} was calculated from the number of reactions with eq. (3.19) displayed as empty circles.

3. k_+^{EC} was obtained form the Erban-Chapman eq. (2.17) and plotted as a dotted line.

concentration of enzymes is a factor 20 smaller than the concentration of substrates. Equations (3.11 - 3.14) were chosen to model the concentrations resulting from the simulation. The microscopic reaction rates and macroscopic reaction rate for a unimolecular reaction should be equal $\lambda_c = k_c$. In eq. (3.11) k_+ was fitted to the sampled concentration. A blue bar in the plot indicates the time window during which the radial distribution was sampled. The corresponding radial distribution will be discussed here after. It was assumed that after $t = 100\Delta t$ steps a stationary distribution was reached. The assumption is based on an approximated constant average number of complexes from there on. The simulation is reproducing the theoretical kinetics. The simulation is not yet reaching equilibrium, with $c_S = 0$ and $c_P = c_{S_0}$, at the end of the simulation. The theoretical results, however, are calculated two decades further.

The next observable of interest is the radial distribution function ($g_{S,E}(\boldsymbol{r})$) of substrates around enzymes. It describes how the conditional density varies as a function of distance ($\boldsymbol{r}$) between enzyme and substrate particles:

$$g_{S,E}(|\boldsymbol{r}|;t) = \frac{1}{N_S(t)N_E(t)}V\sum_{ij}\langle\delta(\boldsymbol{R}_{Si}(t) - \boldsymbol{R}_{Ej}(t) - \boldsymbol{r})\rangle \qquad (3.17)$$

$\boldsymbol{R}_{Sj}(t)$ denotes the position of molecule i of species S at time t and $i = 1, ..., N_S$. In a simulation the radial distribution function can be calculated form the number of substrates $dn(r)$ within an interval $r, r + dr$ away from the enzyme:

$$g_{S,E}(r;t) = \frac{V dn(r)}{N_S(t)N_E(t)4\pi r^2 dr} \qquad (3.18)$$

In a simulation box with periodic boundary conditions, one cannot obtain the structure beyond $r > L/2$. Thus, $g_{S,E}(r;t)$ was sampled in the range $0 < r < 4.0\sigma$ and averaged over the time window ($t = 100\Delta t...819\Delta t$). An ensemble-average of 2544 runs was performed on top. The time-ensemble-average was plotted as green error-bars in fig. 3.2 and compared to Erban-Chapman eqs. (5.19) and (5.20). Again, the simulation is reproducing with good accuracy the radial distribution obtained by eq. (3.18). The radial distribution is deviating from Erban-Chapman only for r close to the enzyme and close to the simulation box boundary. dr was chosen constant. Hence, the volume of the shell decreases for small r, which makes the calculation less accurate for $r \to 0$. That is also the reason for the standard deviation, which is displayed as the error-bars, to increase for $r \to 0$. Erban-Chapman equations are derived by a constant concentration of substrates at infinity. This presumably explains the deviation of the simulation to Erban-Chapmen result close to the boundary of the simulation box. For a better agreement, substrates should be inserted at the boundaries during the simulation to obtain a stationary concentration.

The forward macroscopic reaction rate k_+ was shown by Erban-Chapman to be constant in time for our scenario. In the following k_+ will be obtained by three different ways:

1. From a fit of k_+^{QSSA} in eq. (3.11) to the simulated kinetics.

2. k_+^{EC} from the Erban-Chapman theory with eq. (2.17).

3. From the number of forward reactions dN_{react} of the reaction S + E $\xrightarrow{k_+}$ ES within time interval τ.

$$k_+^{count}(t) = \frac{\langle dN_{react} \rangle}{dt} \frac{1}{V c_S(t) c_E(t)} = \frac{1}{V c_S(t) c_E(t)} \lim_{\tau \to 0} \frac{dN_{react}}{\tau} \qquad (3.19)$$

V is the volume of the simulation box. k_+ was very noisy. A reasonable smooth $k_+(t)$ could be obtained for $\tau = 300\Delta t$. Only the third method calculates the macroscopic forward reaction rate at different times. For the first and second method, k_+ is assumed constant in time. This assumption holds for Brownian motion but not for fractional Brownian motion. The forward reaction rates were calculated with the three methods and plotted as the green in fig. 3.3 for the one-way "Erban-Chapman" scenario. The reaction rate from method 1 and 3 are accurate. They both reproduce similar forward reaction rates. $k_+^{QSSA} = 0.359\sigma^3/\Gamma$ is inside the standard deviation of the mean of $k_+^{count} = (0.360 \pm 0.003)\sigma^3/\Gamma$. The second method rely on a constant concentration of substrates at the boundary. This might cause this method to underestimate the reaction rate $k_+^{EC} = 0.338\sigma^3/\Gamma$. The second method rely solely on the theory and not on the simulation data. The simulation model reproduces the kinetics and spatial distribution of the theoretical results of Erban-Chapman.

"Diffusion-Limited" One-Way Reaction

The following scenario, where the reaction velocity is limited by diffusion will be referred to as the one way "diffusion-limited" scenario. Therefore, diffusion has to be the rate limiting step. However, the microscopic rates cannot be chosen arbitrarily high, due to eq. (2.20). The Microscopic rates $\lambda_+ = 3.0$ and $\lambda_c = 3.0$ were chosen so that the reaction probability $P = 0.15$ during Δt is still a lot smaller than 1. Again, radial distribution function and macroscopic reaction rate forward were sampled analogously to the Erban-Chapman scenario. The resulting radial distribution is shown as blue error-bar in fig. 3.2 and compared to the Erban-Chapmann result 5.19, displayed as a blue solid line. The result, is reproducing the theory very accurately. The macroscopic reaction rate forward is displayed in blue in fig. 3.3. Erban-Chapmans results are underestimating k_+ even more than in the previous scenario. The impact of non-stationary concentrations at the boundaries is probably even stronger for "diffusion-limited" reactions. $k_+^{QSSA} = 2.22\sigma^3/\Gamma$ is inside the standard deviation of the mean of $k_+^{count} = (2.25 \pm 0.08)\sigma^3/\Gamma$ from the counted reaction number.

Subsequently, $1 \leq \lambda_+ \leq 3.0$ was scanned until diffusion becomes the rate limiting step. k_+^{QSSA} was calculated for every simulation. The fastest possible reaction should be limited by eq. (2.14) to be $k_+ = 2.094\sigma^3/\Gamma$. The change of k_+^{QSSA} with λ_+ is displayed in fig. 3.4. Higher reaction rates than the diffusion limit can be observed for $\lambda_+ > 2.0/\Gamma$ presumably because no extra particles were placed at the boundaries, for stationary dynamics.
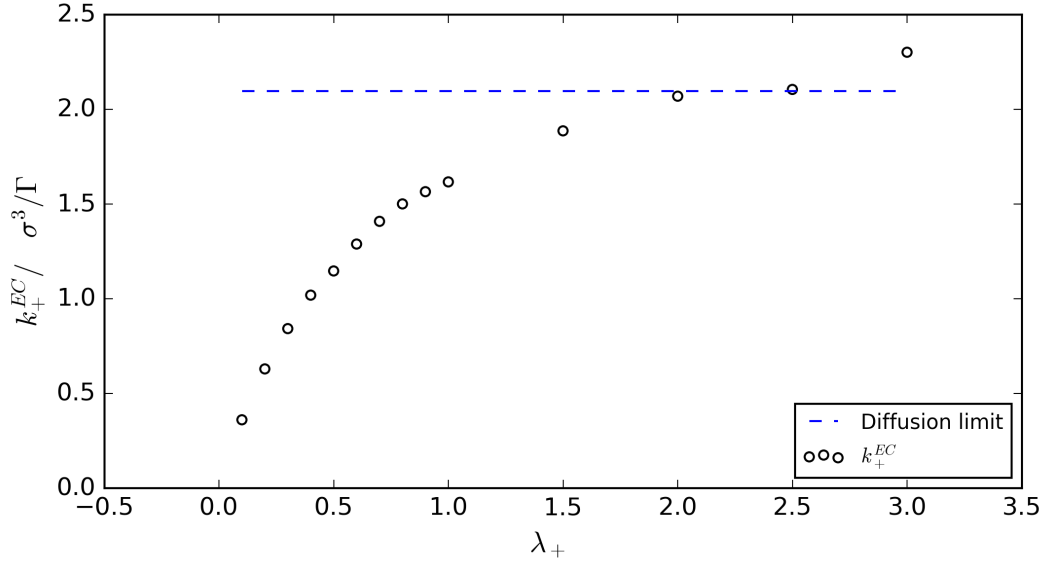
Figure 3.4: The saturation of macroscopic reaction rates with an increase of λ_+ towards a "diffusion-limited" reaction is shown in the plot. k_+^{QSSA} was calculated from simulation data and displayed as empty circles. The dashed blue line describes the diffusion limit eq. (2.14). Microscopic rates were scanned in the range of: $0.1/\Gamma \leq \lambda_+ \leq 3.0/\Gamma$. The remaining microscopic rates were chosen: $\lambda_c = 1.0/\Gamma$, $\lambda_- = 0$.

3.3.2 Michaelis-Menten mechanism

The following scenario will be referred to as the "enzyme blocking" Michaelis-Menten scenario. For "enzyme blocking" Michaelis-Menten, a locally higher concentration of substrates around the enzyme was attempted with $(\lambda_- = 1.0/\Gamma) > (\lambda_c = 0.1/\Gamma)$ and $\lambda_+ = 1.0/\Gamma$. The observables were calculated analogously to the previous scenarios. The concentrations of substrate, enzyme and product are displayed in fig. 3.5 in solid lines. The kinetics of the analogous one-way reaction with same parameters but $\lambda_- = 0.0/\Gamma$ are displayed as a transparent line. Indeed,the blocking is decreasing the reaction velocity (dc_p/dt). Again, equations (3.11 - 3.14) were chosen to model the concentrations resulting from the simulation. They reproduce the simulation accurately. The concentration of complexes is, as expected, higher for the "enzyme blocking" than the one-way scenario. $k_+^{QSSA} = 4.34\sigma^3/\Gamma$, from the fit of eq. (3.11), results in a higher reaction rate than the Erban-Chapman result $k_+^{EC} = 1.25\sigma^3/\Gamma$. Also the method of counting reactions eq. (3.19) yields a comparable macroscopic reaction rate $k_+^{count} = (4.39 \pm 0.02)\sigma^3/\Gamma$. A smaller k_+^{EC} can be presumably explained by a high local concentration of substrates around the enzyme. The radial distribution function was plotted in fig. 3.6 with the Erban-Chapman result as a reference. As expected, the radial distribution shows a higher concentrations of substrates in close proximity to the enzyme.
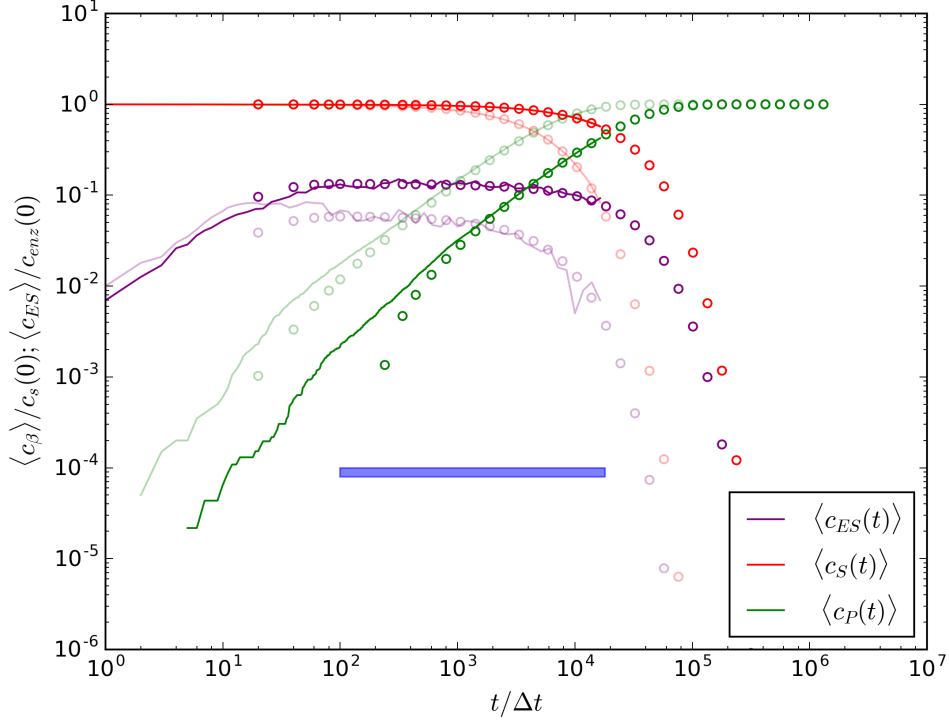
Figure 3.5: Scenario: The "enzyme blocking" Michaelis-Menten reaction with microscopic reactions set to $\lambda_+ = 1$, $\lambda_- = 1$, $\lambda_c = 0.1$ is displayed non-transparently. The "enzyme blocking" scenario is compared to a analogous one-way scenario, which is displayed transparently. Normalised concentrations of substrate, product and complex and their fit (displayed as empty circles) with the QSSA for the substrate concentration are shown. The blue bar in the plot indicates the area where the radial distribution was observed (see fig. 3.6).

3.4 Results for fBm

The mass action law does not hold any more for reactions with fractional Brownian motion. Kopelman suggested for percolation cluster, in which particles diffuse anomalously, time-depended macroscopic reaction rates for bi-molecular reactions of the form: [39]:

$$k(t) = k_0 t^{-h} \qquad \text{for} \qquad 0 \leq h \leq 1 \qquad \text{and} \qquad t \geq 1, \tag{3.20}$$

with h the fractal kinetics exponent. Its value is zero for classic kinetics. For diffusion-limited kinetics in a percolation cluster and a bi-molecular reaction, Kopelman derived a relation between fractal like kinetics exponent h and the spectral
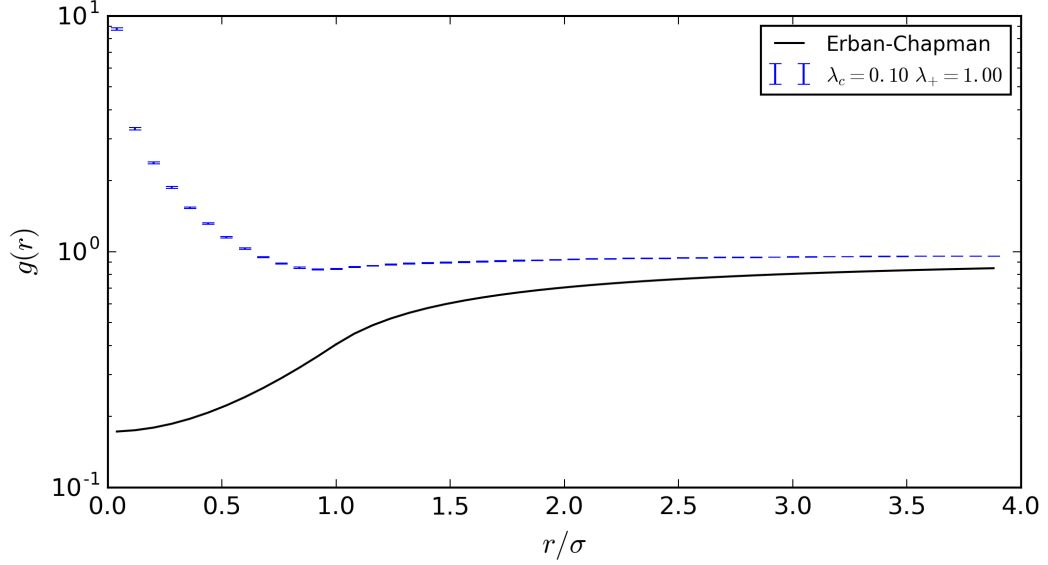
Figure 3.6: Scenario: The "enzyme blocking" Michaelis-Menten reaction with microscopic reactions set to $\lambda_+ = 1$, $\lambda_- = 1$, $\lambda_c = 0.1$. The radial distribution function of "enzyme blocking" scenario of substrates around the enzyme/complex was sampled in the range of $(100\Delta t < t < 2^{14}\Delta t)$ and plotted as error-bars with the width of the standard deviation. The Erban-Chapman 5.19 result was plotted as a solid black line.

dimension d_s:

$$h = 1 - \frac{d_s}{2} \tag{3.21}$$

The spectral dimension is defined by the recurrence probability P of a random walker to return to its origin after time t:

$$P \sim t^{-d_s/2} \tag{3.22}$$

The spectral dimension can be related to the anomalous coefficient $d_s = d \cdot \alpha$, with d the dimension of the space. The fractal exponent h as a result of percolation theory can be related to α for a three-dimensional, diffusion-limited bi-molecular reaction:

$$h = 1 - \frac{3\alpha}{2} \qquad \text{for} \qquad 0 < \alpha < 2/3 \tag{3.23}$$

$$h = 0 \qquad \text{for} \qquad 2/3 < \alpha < 1 \tag{3.24}$$

In the following, kinetics of fractional Brownian motion with $\alpha = 0.5$ have been compared to the same system with normal diffusion $\alpha = 1$. Subsequently, the impact of α on k_+ for one scenario was studied and compared to the theory for percolation cluster mentioned above. The initial densities of substrates $c_{S_0} = 5/128\sigma^3$ and enzymes $c_{E_0} = 1/512\sigma^3$ and diffusion coefficient K_α remained unchanged.
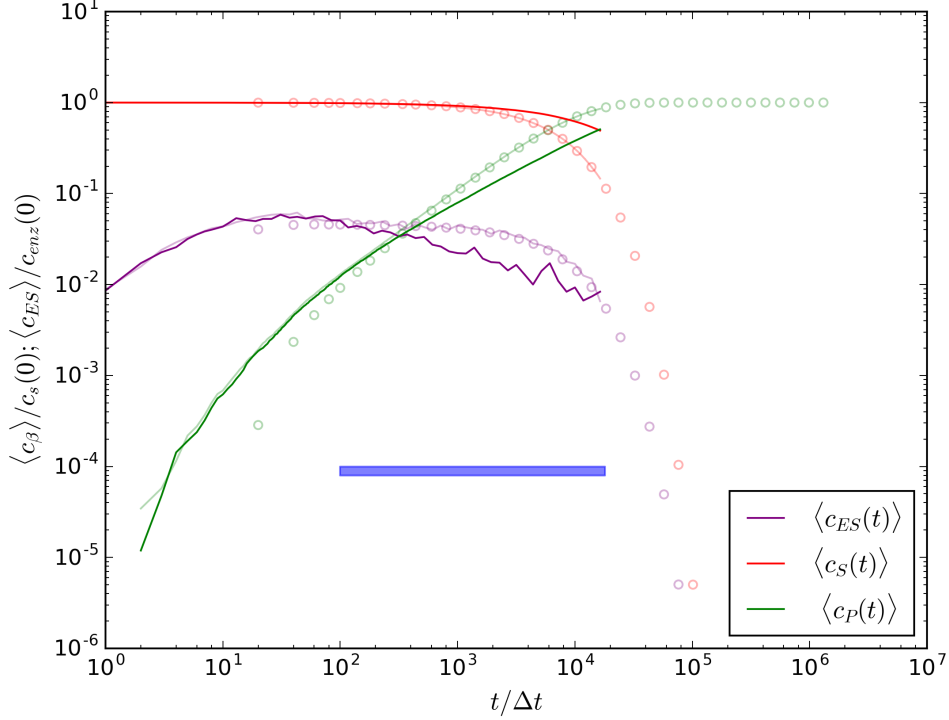
3.4.1 Comparison to Normal Diffusion

Figure 3.7: Scenario: The "fBm-influenced" Michaelis-Menten reaction with microscopic reaction rates set to $\lambda_+ = 1.0$, $\lambda_- = 1.0$, $\lambda_c = 1.0$ and $\alpha = 0.5$ is displayed non-transparently. The "fBm-influenced" scenario is compared to a analogous scenario with $\alpha = 1.0$, which is displayed transparently. Normalised concentrations of substrate, product and complex. For $\alpha = 1.0$ a fit with the QSSA for the substrate concentration are shown as empty circles. The blue bar in the plot indicates the area where the radial distribution was sampled (see fig. 3.8).

The following scenario will be referred to as the "fBm-influenced" Michaelis-Menten scenario. For the "fBm-influenced" sceanrio, microscopic reaction rate ware set to $\lambda_+ = 1.0/\Gamma$, $\lambda_- = 1.0$, $\lambda_c = 1.0/\Gamma$. The kinetics are displayed non-transparently in fig. 3.7. In transparent the same scenario with normal diffusion is plotted. A slowing down of the kinetics compared to normal diffusion is obvious. The concentration of complexes is not constant in time during the time window indicated with a blue bar. Thus, a QSSA ($dc_C/dt = 0$) should not hold. Still, the radial distribution function was sampled in the time window indicated by the blue bar and compared to normal diffusion. The radial distribution function is displayed in fig. 3.8. A stronger depletion of substrates close to the enzyme compared to normal diffusion is present.

A second scenario, referred to as an attempt of fast fBm reactions, with microscopic reaction rates set to $\lambda_+ = 1.0/\Gamma$, $\lambda_- = 1.0$, $\lambda_c = 0.02/\Gamma$ and $\alpha = 0.5$ was
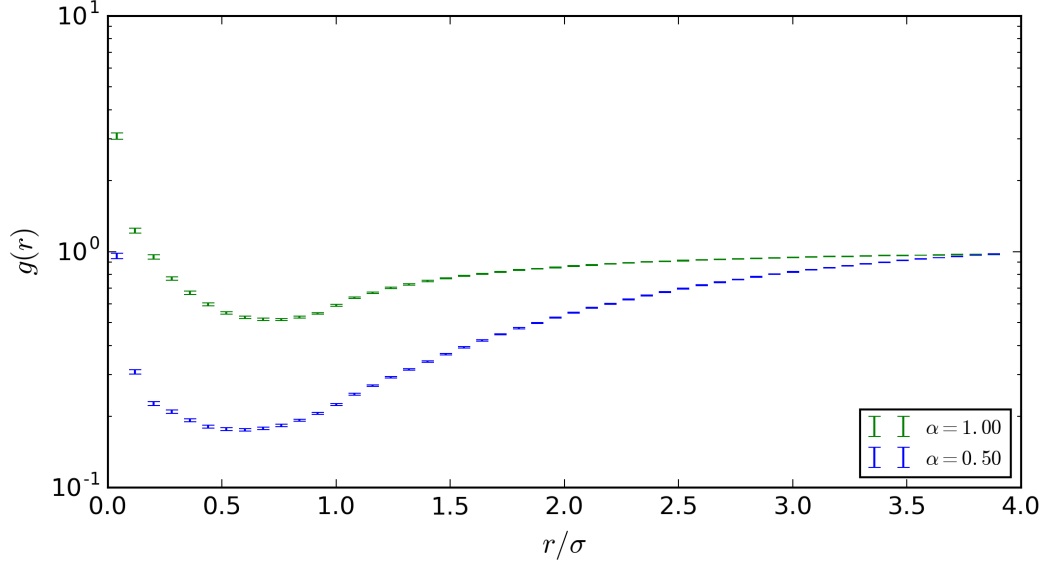
Figure 3.8: The radial distribution function 3.18 of the substrates around the enzyme/complex was sampled in the range of $(100\Delta t < t < 2^{14}\Delta t)$ and plotted as errorbar with the width of the standard deviation and microscopic reaction set to: $\lambda_+ = 1.0/\Gamma$, $\lambda_- = 1.0$, $\lambda_c = 1.0/\Gamma$.
green: Michaelis-Menten reaction: $\alpha = 1.0$
blue: "fBm-influenced" Michaelis-Menten reaction: $\alpha = 0.5$

studied. Intended was a scenario, where kinetics are accelerated due to fBm. With $\lambda_c \gg \lambda_-$, the idea was to increase the density of substrates locally around the enzyme. substrates which propagated with fBm should have more difficulties to escape out of the reaction radius. With similar microscopic reaction rates a higher density of substrates would cause a higher reaction rate. The radial distribution function of an attempt of fast kinetics with fBm is shown in fig. 3.9. The local concentration of substrates around the enzyme is higher for normal diffusion. The impact of slower escape probability is presumably overcompensated by an lower arrival probability of the substrates.
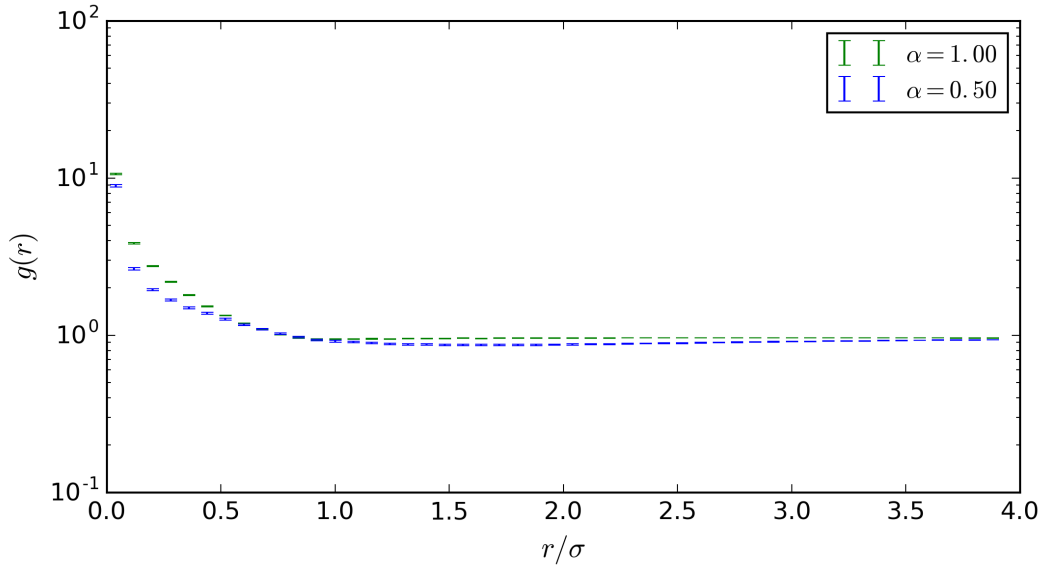
Figure 3.9: Scenario: An attempt of fast fBm reactions. The radial distribution function 3.18 of the substrates around the enzyme/complex was sampled in the range of $(100\Delta t < t < 2^{14}\Delta t)$ and plotted as error-bar with the width of the standard deviation and microscopic reaction set to: $\lambda_+ = 1.0/\Gamma$, $\lambda_- = 1.0$, $\lambda_c = 0.02/\Gamma$.
green: Michaelis-Menten with Bm: $\alpha = 1.0$
blue: Michaelis-Menten with fBm: $\alpha = 0.5$

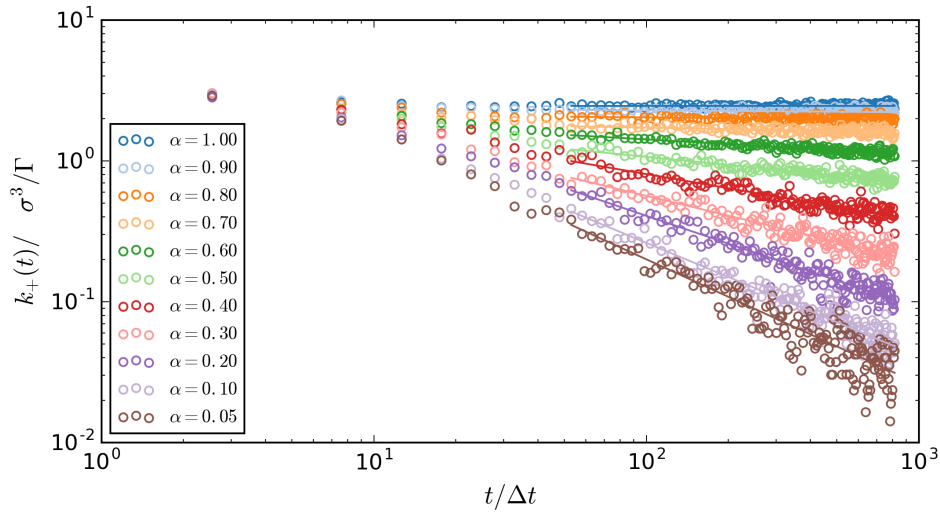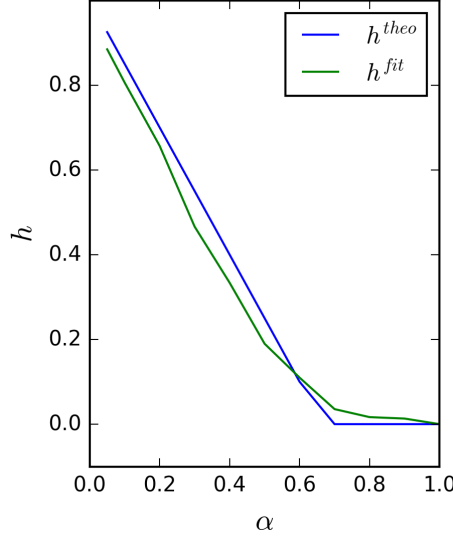### 3.4.2 Fractal Reaction Kinetics

Figure 3.10: Scenario: The "fBm-influenced" Michaelis-Menten reaction with microscopic rates set up to $\lambda_+ = 1.0$, $\lambda_- = 1.0$, $\lambda_c = 1.0$. $k_+^{count}(t)$ was sampled and displayed as empty circles in the range of $0.05 \leq \alpha \leq 1.0$. With eq. (3.20), the fractal like kinetics exponent h was fitted and plotted as solid lines.

α	$h^{fit}(\alpha)$	$h^{theo}(\alpha)$
0.05	0.88441	0.925
0.1	0.80584	0.85
0.2	0.65659	0.7
0.3	0.46603	0.55
0.4	0.33364	0.4
0.5	0.18971	0.25
0.6	0.10969	0.1
0.7	0.03544	0.0
0.8	0.01657	0.0
0.9	0.01320	0.0
1.0	0.0	0.0

Figure 3.11 & Table 3.1: Impact of α on h resulting from a fit (h^{fit}) of the simulations displayed in fig. 3.10 and from the percolation theory (h^{theo}).

As suggested by the theory for a "diffusion limited" bi-molecular reaction in a percolation cluster, the reaction rate should become time-depended for $\alpha > 2/3$ eq. (3.23). The impact of α on $k_+^{count}(t)$ was simulated for a "fBm-influenced" Michaelis-Menten reaction with microscopic reaction rates $\lambda_+ = 1.0$, $\lambda_- = 1.0$, $\lambda_c = 1.0$. $k_+^{count}(t)$ for $0.05 > \alpha > 1$ was averaged over at least 2400 runs and displayed in fig. 3.10. The fractional kinetics exponent h^{fit} was fitted via eq. (3.20) and plotted as solid lines into the figure. h^{fit} and h^{theo} from the theory have been compared in fig. 3.11. Theory, although formulated for percolation cluster, and simulation are in good agreement.

3.5 Conclusion

The simulation model is capable of reproducing the theoretical results of Smoluchwoski and Erban-Chapman for a bi-molecular one-way reaction S + E $\xrightarrow{k_+}$ ES $\xrightarrow{k_c}$ P + E. The "diffusion-limited" scenario revealed the strongest deviations from theory. However, in theory a constant concentration of substrates is assumed at $r \to \infty$, which is not included in the simulation model. The simulation model can also be described by Michaelis-Menten kinetics with a QSSA for $c_S(t)$ and normal diffusion. The initial concentration of substrates was chosen a factor 20 higher than the concentration of enzymes. Thus, the QSSA is applicable. From theory, QSSA holds for $c_{S_0} \gg c_{E_0}$. The "enzyme-blocking" Michaelis-Menten scenarios results in locally higher concentration of substrates around the enzyme in comparison to the one-way reactions. Scenarios with normal diffusion, with available theory as a reference, deal as a validation of the simulation model. A good agreement of theory and simulation model was shown. In the following Michaelis-Menten scenarios with fractional mo-

tion were simulated. No scenario of faster reaction kinetics due to fBm was found, but all simulations in a diffusion-influenced regime were of fractal type. The impact of slower escape probability on kinetics is presumably overcompensated by an lower arrival probability of the substrates. A stronger depletion of substrates around enzymes for fBm in comparison to Bm was observed. From percolation theory of a "diffusion-controlled" bi-molecular reaction, the fractal kinetics exponent, was compared with good agreement to results generated by the simulation in the range of $0.05 < \alpha < 1.0$. Anomalous coefficients smaller than $\alpha < 0.5$ are unusual in nature, however, they are of theoretical interest. These results validate our implementation of fBm in RevReaDDy.

4 Summary

In cells, reaction-diffusion simulations are particularly challenging. On one hand, large numbers of macromolecules densely packed cause classical particle-based simulations to reach computational limits very early. On the other hand, small molecular abundances of particular species cause simulations based on a "well-mixed assumption" to be inaccurate, although computationally favourable. For a specific reaction-diffusion system, only specific reactions are of interest. Most of the molecules, thereby, are not involved in reactions but induce anomalous diffusion. The aim of this thesis is to tackle the impact of anomalous diffusion on reaction-diffusion systems for an enzymatic reaction.

Diffusion was chosen to be modelled by fractional Brownian motion. This approach approximates the influence of the crowded biological medium by long-range correlations of the trajectory increments. First, theoretical foundations for fBm were set. Most importantly auto-covariance functions for fractional Brownian noise and motion were introduced. Subsequently, fBm-generating algorithms were studied in terms of accuracy and performance. They rely on the Wiener-Khintchin's theorem and the auto-covariance functions introduced beforehand. A naive, Cholesky, Davis-Harte and Lowen fBm-generating algorithms were implemented and analysed in terms of accuracy and performance. Our implementation of Lowen algorithm turned out not to be exact as claimed by the author[14]. A slightly modified version of Lowen algorithm was introduced. The modified version turned out to overcome the problem of a non-Gaussian distribution. Davis-Harte and modified Lowen algorithms seem to be both, exact and fast $\mathcal{O}(Mlog(M))$ with the trajectory length (M).

The influence of diffusion on kinetics was studied. Uni-molecular reactions are not influenced by diffusion and elementary tri-molecular reactions are negligible according to collision theory. Thus, bi-molecular reactions were studied. The Smoluchwoski result for "diffusion-limited" and the Erban-Chapman result for "diffusion-influenced" bi-molecular reactions were derived. Along the way, the law of mass action was shown to follow for stationary dynamics, no particle interaction and normal diffusion. The theoretical results from Erban-Chapman motivate a particle-based simulation model for bi-molecular reactions in RevReaDDy. RevReaDDy is a PBRD tool developed by Christoph Fröhner within his PhD project. Conventionally, particles propagate with Bm in RevReaDDy. In the process of the thesis, RevReaDDy was extended by fractional Brownian motion, by Davis-Harte and modified Lowen algorithm. The algorithm analysis suggests Davis-Harte and modified Lowen algorithm to be most promising for an implementation. However, forces are not included in the fBm implementation. Both algorithms generate all increments beforehand, which caused is the major modification of RevReaDDy during implementation. In

the process of implementation, further modifications to RevReaDDy were necessary to address.

fBm is modelling the motion in a crowded biological environment. Enzymatic reactions are biologically very relevant and occur in anomalous environments, modelled by fBm. In fact, biochemical reactions are controlled mainly by enzymes. The most common description of enzyme reactions is given by the Michaelis-Menten mechanism. The theoretical foundation of the Michaelis-Menten mechanism was studied, especially the reaction kinetics in a quasi-steady state approximation. A simulation model of the MM mechanism was implemented into RevReaDDy.

Various scenarios in our simulation model of MM mechanism were studied. The size of the simulation box, initial concentrations of the reactants, diffusion coefficients and reaction distance were fixed and not varied for all scenarios. The initial concentration of substrates was chosen a factor 20 higher than the concentration of enzymes. Thus, the QSSA is applicable. Microscopic reaction rates and the anomalous diffusion coefficient α were varied for different scenarios. First, it was shown, that the simulation model is indeed capable of reproducing theoretical results in "diffusion-influenced" and "diffusion-limited" one-way reactions for normal diffusion. One-way means no back reaction from the complex to substrate and enzyme. The kinetics and radial distribution function are in good agreement with the theory, although small deviations to the theory can be explained presumably by nonconstant concentration at the simulation box boundary. The theory is derived under the assumption of a constant concentration of substrates at infinity. Subsequently, an MM reaction with strong enzyme blocking was studied. The kinetics are in good agreement with the theory of the MM mechanism. Scenarios with normal diffusion, with available theory as a reference, deal as a validation of the simulation model. Eventually, the MM mechanism with fractional Brownian motion was studied. No scenario with enhanced kinetics due to fBm was found, but all simulations in a "diffusion-controlled" regime were of fractal type. The fractal kinetics exponent was shown to well agree with the theory for "diffusion-limited" bi-molecular reactions in percolation cluster.

As an outlook of the thesis, forces could be implemented into RevReaDDy's fBm extension. Although, an fBm algorithm with possible potentials included will probably be very slow. It could be of interest to extend the implementation not only to model fBm but to model a motion measured by an experiment. Therefore, the velocity auto-correlation function from fBm should by replaced by a VACF measured by an experiment.

5 Appendix

5.1 From Central Limit Theorem to Gaussian Distribution

In the following the Central Limit Theorem will be applied to calculated the distribution of Y, $\rho(y)dy = P(y < Y < y + dy)$ in the limit of large N, with Y being defined as the sum of an random variable:

$$Y = \frac{1}{\sqrt{N}} \sum_{j=1}^{N} X_j \tag{5.1}$$

The Generating function for a random variable Y is:

$$G_Y(k) = \langle e^{ikY} \rangle = \int e^{ikY} \rho(y)dy \tag{5.2}$$

eq. (5.1) can be inserted into the generating function, which results in:

$$G_Y(k) = \langle e^{\frac{ik}{\sqrt{N}} \sum_{j=1}^{N} X_j} \rangle$$

$$G_Y(k) = \langle \prod_{j=i}^{N} e^{\frac{ik}{\sqrt{N}} X_j} \rangle$$

If all X_j are independent, then:

$$G_Y(k) = \prod_{j=i}^{N} \langle e^{\frac{ik}{\sqrt{N}} X_j} \rangle = e^{\sum_{j=1}^{N} A_j(\frac{k}{\sqrt{N}})} \tag{5.3}$$

$$\text{with } A_j(\frac{k}{\sqrt{N}}) = ln\langle e^{\frac{ik}{\sqrt{N}} X_j} \rangle$$

For large N behavior, we assume $\frac{k}{\sqrt{N}} << 1$ and expand

$$A_j(\frac{k}{\sqrt{N}}) = ln(1 + \langle X_j \rangle \frac{ik}{\sqrt{N}} - \langle X_j^2 \rangle \frac{k^2}{2N} + \mathcal{O}(N^{-\frac{3}{2}})) \tag{5.4}$$

with a finite variance $\sigma_i^2 = \langle X_i^2 \rangle$ and the mean $\langle X_i \rangle = 0$

$$A_j(\frac{k}{\sqrt{N}}) = -\sigma_j^2 \frac{k^2}{2N} + \mathcal{O}(N^{-\frac{3}{2}})) \tag{5.5}$$

Thus, the generating function for large N is:

$$G_Y(k) = e^{-\frac{\sigma^2 k^2}{2}} \tag{5.6}$$

$$\text{with } \sigma = \frac{1}{N}\sum_{j=1}^{N}\sigma_j^2$$

The distribution of Y can be calculated via the inverse Fourier Transform:

$$\rho(y) = \frac{1}{2\pi}\int_{-\infty}^{\infty} e^{-\frac{\sigma^2 k^2}{2}} e^{iky} dk \tag{5.7}$$

$$= \frac{1}{\sqrt{2\pi}\sigma} e^{-\frac{y^2}{2\sigma^2}} \tag{5.8}$$

$\rho(y)$ results in a Gaussian distribution.

5.2 From Gaussian Distribution to Gaussian Transition Probability

The conditional distribution function to be in x at time t if visited position y at time s can be written due to Bayes' theorem as a transition probability from y to x in time $t - s$ multiplied with the probability to be in y at time s:

$$\rho_{t,s}(x,y) = T_{t-s}(x|y)\rho_s(y) \tag{5.9}$$

Further due to particle conservation another relation holds:

$$\rho_t(x) = \int \rho_{t,s}(x,y)dy \tag{5.10}$$

Having an initial condition $\rho_s(x) = \delta(x - y)$:

$$\rho_{t,s}(x|y) = \int \rho_{t,s}(x,y)dy = \int T_{t-s}(x|y)\rho_s(y)dy \tag{5.11}$$

$$= \int T_{t-s}(x|y)\delta(x-y)dy = T_{t-s}(x|y) \tag{5.12}$$

5.3 Einstein Formula

The derivative of the mean variance of the Gaussian distribution in respect to time is defined as:

$$\frac{d}{dt}\delta \boldsymbol{r}^2(t) = \frac{d}{dt}\langle\Delta \boldsymbol{R}^2(t)\rangle = \frac{d}{dt}\int d\boldsymbol{r}\boldsymbol{r}^2 c(\boldsymbol{r},t) = \int d\boldsymbol{r}\boldsymbol{r}^2 \frac{\partial}{\partial t}c(\boldsymbol{r},t) \tag{5.13}$$

Fick's second law can be applied:

$$= D \int_{-\infty}^{\infty} d\boldsymbol{r} r^2 \Delta c(\boldsymbol{r}, t) \tag{5.14}$$

Assuming a reasonable assumption $c(\pm\infty, t) = 0$ and two times partial integration one can derive:

$$= -2D \int_{-\infty}^{\infty} d\boldsymbol{r} \boldsymbol{r} \nabla c(\boldsymbol{r}, t) \tag{5.15}$$

$$= 2Dd \int_{-\infty}^{\infty} d\boldsymbol{r} c(\boldsymbol{r}, t) = 2dD \tag{5.16}$$

For the initial condition $\boldsymbol{r}(0) = 0$, one gets the Einstein Formula: $\langle (\boldsymbol{r}(t) - \boldsymbol{r}(0))^2) \rangle = 2dDt$

5.4 Erban-Chapman

The calculation can be started from eq. (2.8). This derivation can be found in [27]. The stationary distribution can be written as:

$$\left(\frac{\partial}{\partial_r} + \frac{2}{r} \right) D \frac{\partial \rho_t(r)}{\partial_r} = 0 \qquad \text{for} \qquad r \geq \sigma \tag{5.17}$$

$$\left(\frac{\partial}{\partial_r} + \frac{2}{r} \right) D \frac{\partial \rho_t(r)}{\partial_r} = \lambda_+ \rho_t(r) \qquad \text{for} \qquad r \leq \sigma \tag{5.18}$$

For $r \leq \sigma$ a production term had been added to the continuity equation. The general solution can be written as:

$$\rho_t(r) = a_1 + \frac{a_2}{r} \qquad \text{for} \qquad r \geq \sigma \tag{5.19}$$

$$\rho_t(r) = \frac{a_3}{r} \exp \left[r \sqrt{\frac{\lambda_+}{D}} \right] + \frac{a_4}{r} \exp \left[-r \sqrt{\frac{\lambda_+}{D}} \right] \qquad \text{for} \qquad r \leq \sigma \tag{5.20}$$

with a_1, a_2, a_3, a_4 real constants. Just like in the calculation in diffusion limit the distribution at $r \to \infty$ is defined as the concentration of particle A $\rho_t(r \to \infty) = C_A$. Thus $a_1 = C_A$ and due to the continuity of the density distribution , $a_3 = -a_4$. Further, due to the continuity of the the flux $j_s(r)$ at $r = \sigma$ also a_2 and a_3 can be determined:

$$a_2 = C_A \left(\sqrt{\frac{D}{\lambda_+}} \tanh \left(\sigma \sqrt{\frac{\lambda_+}{D}} \right) - \sigma \right) \tag{5.21}$$

$$a_3 = \frac{C_A \sqrt{\frac{D}{\lambda_+}}}{2 \cosh \left(\sigma \sqrt{\frac{\lambda_+}{D}} \right)} \tag{5.22}$$

The flux at $r = \sigma$ can be written as:

$$j^s(\sigma) = D\frac{\partial \rho_t(\sigma)}{\partial_\sigma} = -D\frac{a_2}{\sigma^2} \tag{5.23}$$

Gauss's theorem states that the negative flux of a quantity through a closed surface is equal to the production of that quantity inside the volume. Further The change of complex AB is proportional to the change of A inside the volume of of the sphere with $r = \sigma$. The total flux and thus the change of AB can be written as:

$$\frac{dC_{AB}}{dt} = -\int_{\partial V} j^s(\sigma)da = \int_{\partial V} D\frac{a_2}{\sigma^2}da = -4\pi D a_2 C_B \tag{5.24}$$

$$= 4\pi D C_B C_A \left(\sigma - \sqrt{\frac{D}{\lambda_+}}\tanh\left(\sigma\sqrt{\frac{\lambda_+}{D}}\right)\right) \tag{5.25}$$

Bibliography

[1] A. P. Minton: *How can Biochemical Reactions Within Cells Differ From Those in Test Tubes?*, Journal of cell science **119**, 2863 (2006).

[2] F. Höfling and T. Franosch: *Anomalous Transport in the Crowded World of Biological Cells*, Reports on Progress in Physics **76**, 046602 (2013).

[3] B. B. Mandelbrot and J. W. Van Ness: *Fractional Brownian Motions, Fractional Noises and Applications*, SIAM Review **10**, 422 (1968).

[4] L. Michaelis and M. L. Menten: *Die kinetik der invertinwirkung*, Biochem. z **49**, 352 (1913).

[5] R. Huang, I. Chavez, K. M. Taute, B. Lukić, S. Jeney, M. G. Raizen, and E.-L. Florin: *Direct observation of the full transition from ballistic to diffusive brownian motion in a liquid*, Nature Physics **7**, 576 (2011).

[6] F. Höfling: *Stochastic processes and correlation functions*, University Lecture (2016).

[7] A. Fick: *On liquid diffusion*, Poggendorffs Annalen (1855).

[8] J. Fourier: *Theorie Analytique de la Chaleur* (Firmin Didot, 1822).

[9] A. Einstein: *Über die von der molekularkinetischen theorie der wärme geforderte bewegung von in ruhenden flüssigkeiten suspendierten teilchen*, Annalen der Physik **322**, 549 (1905).

[10] M. von Smoluchowski: *Zur kinetischen theorie der brownschen molekularbewegung und der suspensionen*, Annalen der Physik **326**, 756 (1906).

[11] H. Qian: *Fractional brownian motion and fractional gaussian noise*, in *Processes With Long-Range Correlations* (Springer, 2003), pp. 22–33.

[12] T. Dieker: *Simulation of Fractional Brownian Motion*, Master's thesis (2004).

[13] J. R. M. Hosking: *Modeling persistence in hydrological time series using fractional differencing*, Water Resources Research **20**, 1898 (1984).

[14] S. B. Lowen: *Efficent generation of fractional brownian motion for simulation of infrared focal-plane array calibration drift*, Methodology And Computing In Applied Probability **1**, 445 (1999).

[15] R. B. DAVIES and D. S. HARTE: *Tests for hurst effect*, Biometrika **74**, 95 (1987).

[16] M. Timmer, J.;Koenig: *On generating power law noise*, Astronomy and Astrophysics **300**, 707 (1995).

[17] *Fftw*, http://www.fftw.org/ (Accessed: 20.11.2016).

[18] M. Matsumoto and T. Nishimura: *Mersenne twister: a 623-dimensionally equidistributed uniform pseudo-random number generator*, ACM Transactions on Modeling and Computer Simulation **8**, 3 (1998).

[19] P. Horvai, T. Komorowski, and J. Wehr: *Finite time approach to equilibrium in a fractional brownian velocity field*, Journal of Statistical Physics **127**, 553 (2007).

[20] P. Waage and C. M. Gulberg: *Studies concerning affinity*, Journal of Chemical Education **63**, 1044 (1986).

[21] R. Erban, J. Chapman, and P. Maini: *A practical guide to stochastic simulations of reaction-diffusion processes* (2007).

[22] D. T. Gillespie: *Exact stochastic simulation of coupled chemical reactions*, The Journal of Physical Chemistry **81**, 2340 (1977).

[23] S. Winkelmann and C. Schütte: *The spatiotemporal master equation: Approximation of reaction-diffusion dynamics via markov state modeling*, The Journal of Chemical Physics **145**, 214107 (2016).

[24] J. Schöneberg, A. Ullrich, and F. Noé: *Simulation tools for particle-based reaction-diffusion dynamics in continuous space*, BMC Biophysics **7** (2014).

[25] G. Gruenert, B. Ibrahim, T. Lenser, M. Lohel, T. Hinze, and P. Dittrich: *Rule-based spatial modeling with diffusing, geometrically constrained molecules*, BMC Bioinformatics **11**, 307 (2010).

[26] M. v. Smoluchowski: *Versuch einer mathematischen Theorie der Koagulationskinetik kolloider Lösungen* (1917).

[27] R. Erban and S. J. Chapman: *Stochastic modelling of reaction–diffusion processes: Algorithms for bimolecular reactions*, Physical Biology **6**, 046001 (2009).

[28] M. B. Flegg: *Smoluchowski Reaction Kinetics for Reactions of any Order* pp. 1–30 (2015).

[29] J. Schöneberg and F. Noé: *Readdy - a software for particle-based reaction-diffusion dynamics in crowded cellular environments*, PLOS ONE **8**, 1 (2013).

[30] The HDF Group: *Hierarchical Data Format, version 5* (1997-NNNN), /HDF5/.

[31] R. Wolfenden and M. J. Snider: *The depth of chemical time and the power of enzymes as catalysts*, Accounts of Chemical Research **34**, 938 (2001).

[32] H. Berry: *Monte Carlo Simulations of Enzyme Reactions in two Dimensions: Fractal Kinetics and Spatial Segregation.*, Biophysical journal **83**, 1891 (2002).

[33] S. Schnell and T. E. Turner: *Reaction Kinetics in Intracellular Environments With Macromolecular Crowding: Simulations and Rate Laws*, Progress in Biophysics and Molecular Biology **85**, 235 (2004).

[34] T. E. Turner, S. Schnell, and K. Burrage: *Stochastic Approaches for Modelling in Vivo Reactions*, Computational Biology and Chemistry **28**, 165 (2004).

[35] J.-H. Jeon, A. V. Chechkin, and R. Metzler: *First passage behavior of multi-dimensional fractional brownian motion and application to reaction phenomena*, in *First-Passage Phenomena and Their Applications* (World Scientific ,City, 2014), pp. 175–202.

[36] G. E. Briggs and J. B. S. Haldane: *A note on the kinetics of enzyme action*, Biochemical Journal **19**, 338 (1925).

[37] B. O. Palsson: *On the dynamics of the irreversible michaelis-menten reaction mechanism*, Chemical Engineering Science **42**, 447 (1987).

[38] S. Schnell and C. Mendoza: *Closed form solution for time-dependent enzyme kinetics*, Journal of Theoretical Biology **187**, 207 (1997).

[39] R. Kopelman: *Fractal reaction kinetics*, Science **241**, 1620 (1988).

Selbstständigkeitserklärung

Hiermit erkläre ich, dass ich die vorliegende Arbeit selbstständig angefertigt, nicht anderweitig zu Prüfungszwecken vorgelegt und keine anderen als die angegebenen Hilfsmittel verwendet habe. Sämtliche wissentlich verwendete Textausschnitte, Zitate oder Inhalte anderer Verfasser wurden ausdrücklich als solche gekennzeichnet.

Jan Grzegorzewski, 21.12.2016   . . . .
                                        Unterschrift